(2)

PIEZOELECTRIC AND ELECTROSTRICTIVE MATERIALS FOR TRANSDUCERS APPLICATIONS

Period February 1, 1991 to January 31, 1992

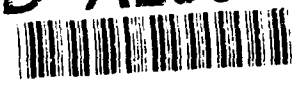

Final Report

VOLUME IV

OFFICE OF NAVAL RESEARCH
Contract No. N00014-89-J-1689

APPROVED FOR PUBLIC RELEASE – DISTRIBUTION UNLIMITED

L. E. Cross
R. E. Newnham
A. S. Bhalla
J. P. Dougherty
J. H. Adair
V. K. Varadan
V. V. Varadan

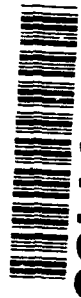

PENNSTATE

THE MATERIALS RESEARCH LABORATORY
UNIVERSITY PARK, PA

SECURITY CLASSIFICATION OF THIS PAGE

REPORT DOCUMENTATION PAGE

Form Approved
OMB No. 0704-0188

1a. REPORT SECURITY CLASSIFICATION	1b. RESTRICTIVE MARKINGS
2a. SECURITY CLASSIFICATION AUTHORITY	3. DISTRIBUTION/AVAILABILITY OF REPORT Reproduction in whole or in part is permitted for any purpose of the United States Governmer
2b. DECLASSIFICATION/DOWNGRADING SCHEDULE	
4. PERFORMING ORGANIZATION REPORT NUMBER(S) N00014-89-J-1689	5. MONITORING ORGANIZATION REPORT NUMBER(S)
6a. NAME OF PERFORMING ORGANIZATION MATERIALS RESEARCH LABORATORY 6b. OFFICE SYMBOL (If applicable)	7a. NAME OF MONITORING ORGANIZATION
6c. ADDRESS (City, State, and ZIP Code) THE PENNSYLVANIA STATE UNIVERSITY UNIVERSITY PARK, PA 16802	7b. ADDRESS (City, State, and ZIP Code)
8a. NAME OF FUNDING/SPONSORING ORGANIZATION 8b. OFFICE SYMBOL (If applicable)	9. PROCUREMENT INSTRUMENT IDENTIFICATION NUMBER
8c. ADDRESS (City, State, and ZIP Code)	10. SOURCE OF FUNDING NUMBERS PROGRAM ELEMENT NO. / PROJECT NO. / TASK NO. / WORK UNIT ACCESSION NO.

11. TITLE (Include Security Classification)
PIEZOELECTRIC AND ELECTRO[illegible]ICTIVE MATERIALS FOR TRANSDUCER APPLICATIONS

12. PERSONAL AUTHOR(S)
L. E. Cross, R. E. Newnham, A. S. Bhalla, J. P. Dougherty, J. H. Adair, V.K. Varadan, V.V.Vara

13a. TYPE OF REPORT	13b. TIME COVERED	14. DATE OF REPORT (Year, Month, Day)	15. PAGE COUNT
FINAL	FROM 2/1/91 TO 1/31/92		

16. SUPPLEMENTARY NOTATION

17. COSATI CODES			18. SUBJECT TERMS (Continue on reverse if necessary and identify by block number)
FIELD	GROUP	SUB-GROUP	

19. ABSTRACT (Continue on reverse if necessary and identify by block number)

SEE REVERSE SIDE OF PAGE.

20. DISTRIBUTION/AVAILABILITY OF ABSTRACT	21. ABSTRACT SECURITY CLASSIFICATION
☐ UNCLASSIFIED/UNLIMITED ☐ SAME AS RPT. ☐ DTIC USERS	
22a. NAME OF RESPONSIBLE INDIVIDUAL	22b. TELEPHONE (Include Area Code) / 22c. OFFICE SYMBOL

DD Form 1473, JUN 86 Previous editions are obsolete. SECURITY CLASSIFICATION OF THIS PAGE

ABSTRACT

This report documents work carried out in the Materials Research Laboratory of The Pennsylvania State University on the third and final year of the program on "Piezoelectric and Electrostrictive Materials for Transducers Applications" sponsored by the Office of Naval Research (ONR) under grand No. N00014-89-J-1689. This marks the termination of a very long and highly productive sequence of contracts and grants focusing on the development of new materials for Piezoelectric and Electrostrictive transducer applications carried through under core ONR funding. Fortunately many elements of the work will be continuing on a new University Research Initiative (URI) program under ONR sponsorship.

Highlights of the past year's activities include: An increased emphasis upon the flextensional (moonie) type actuators, modeling both the internal stress distribution as a function of geometry, and the very interesting resonant mode structure of the composites; A more refined focus upon the performance of piezoelectric ceramic transducers, particularly under high drive levels is developing with concern for the extrinsic domain and phase boundary contributions to response. Measurement and modelling are being used to explore the nonlinearity and the frequency response and to examine the phase partitioning at the rhombohedral : tetragonal morphotropic phase boundary in the PZT system. Phenomena limiting lifetime in polarization and phase switching actuators are being explored to separate surface and volume effects and those due to grain size and flaw population differences. New work has been initiated to examine Acoustic Emission as a technique, in combination with Barkhausen current pulse analysis, to separate and evaluate domain switching and microcracking in polarization switching systems.

From work on this program it has now become clear that the relaxor ferroelectrics are in fact close analogues of the magnetic spin glasses, so that the spin glass formalism can be used to explain the very wide range of dielectric, elastic and electrostrictive properties. The remaining outstanding fundamental problem is that of the detailed interrelationship between the known nano-heterogeneity in the structure and chemistry and the nanopolar regions which contribute the electrical response.

Of very high practical interest is the manner in which the relaxor can be field biased into extremely strong piezoelectric response. Work is going forward to examine this response in detail and to explore the possibility that such "super-responses' can be induced by chemical (solid solution) means.

Processing studies have focused upon new lower temperature consolidations for relaxors, and upon new compositions for high temperature piezoelectric ceramics.

In parallel with the ONR Transducer Program the Laboratory has extensive DARPA sponsored research on ferroelectric thin films. Since the films structures frequently involve materials like the PZT, PMN : PT, PLT and PLZT families of compositions and do explore piezoelectric effects and applications, a small group of the most relevant papers form this program are appended to the report.

PIEZOELECTRIC AND ELECTROSTRICTIVE MATERIALS FOR TRANSDUCERS APPLICATIONS

Period February 1, 1991 to January 31, 1992

Final Report

VOLUME IV

OFFICE OF NAVAL RESEARCH
Contract No. N00014-89-J-1689

APPROVED FOR PUBLIC RELEASE – DISTRIBUTION UNLIMITED

L. E. Cross
R. E. Newnham
A. S. Bhalla
J. P. Dougherty
J. H. Adair
V. K. Varadan
V. V. Varadan

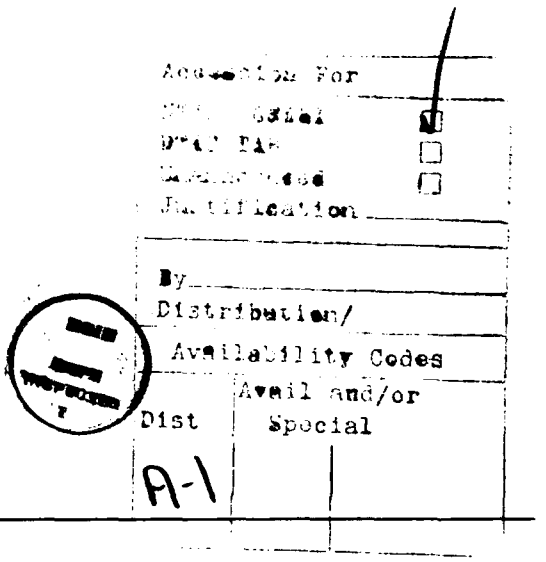

PENNSTATE

1855

THE MATERIALS RESEARCH LABORATORY
UNIVERSITY PARK, PA

TABLE OF CONTENTS

APPENDICES

General Summary Papers

1. L. Eric Cross. "Ferroelectric Ceramics Tailoring Properties for Specific Applications."

2. R. E. Newnham and T. R. Shrout. "Advanced Ceramics," Electronic Ceramics 1, 601-620.

Composite Materials

3. R. E. Newnham "Tunable Transducers: Nonlinear Phenomena in Electroceramics," National Institute of Standards and Technology Special Publication 804, Chemistry of Electonic Ceramic Materials, Proceedings of the International Conference held in Jackson, WY, August 17-22, 1990, issued January 1991.

4. R. E. Newnham. "Composite Electroceramics," International Encyclopedia of Composites, Vol. 6, 158-173.

TABLE OF CONTENTS
(continued)

Composite Materials (continued)

Piezoelectric Ceramics

Phenomenological Studies

TABLE OF CONTENTS
(continued)

Phenomenological Studies (continued)

Relaxors and Related Systems

TABLE OF CONTENTS
(continued)

Processing Studies

31. V. Srikanth and E. C. Subbarao. "Chemical Reactions of Lead Magnesium Niobate Titanate in the Presence of a Glass," J. Mater. Res. **6** (6), 1-16 (June 1991).

32. Paul A. Fuierer and Robert E. Newnham. "$La_2Ti_2O_7$ Ceramics," J. Am. Ceram. Soc. **74** (11), 2876-2881 (1991).

33. G. R. Fox, J. H. Adair and R. E. Newnham. "Effects of pH and H_2O_2 Upon Coprecipitated $PbTiO_3$ Powders," J. Mater. Sci. **26**, 1187-1191 (1991).

34. G. A. Rossetti, Jr., D. J. Watson, R. E. Newnham and J. H. Adair. "Kinetics of the Hydrothermal Crystallization of the Perovskite Lead Titantae," J. Crystal Growth **116**, 251-259 (1992).

35. A. Srivastava, A. Bhalla and L. E. Cross. "A Study of $Y_1Ba_2Cu_3O_{7-x}$ Thick Films on Ferroelectric Substrates."

36. A. Srivastava, A. Bhalla and L. E. Cross. "$Y_1Ba_2Cu_3O_{7-x}$ As An Electrode Materials for Ferroelectric Devices," Ferroelectrics **123**, 243-251 (1991).

Ferroelectric Thin Films

37. K. R. Udayakumar, J. Chen, P. J. Schuele, L. E. Cross, V. Kumar and S. B. Krupanidhi. "Polarization Reversal and High Dielectric Permittivity in Lead Magnesium Niobate Titanate Thin Films," Appl. Phys. Lett. **60** (10), 1187-1189 (9 March 1992).

38. K. R. Udayakumar, P. J. Schuele, J. Chen, K. G. Brooks and L. E. Cross. "Ferroelectric Switching in Lead Zirconate-Lead Zinc Niobate Thin Films."

39. Keith G. Brooks, Jiayu Chen, K. R. Udayakumar and L. Eric Cross. "Lead Zirconate Titanate Stannate Thin Films for Large Strian Microactuator Applications."

40. K. R. Udayakumar, S. F. Bart, A. M. Flynn, J. Chen, L. S. Tavrow, L. E. Cross, R. A. Brooks, D. J. Ehrlich. "Ferroelectric Thin Film Ultrasonic Micromotors," IEEE, 109-113 (1991).

41. Anita M. Flynn, Lee S. Tavrow, Stephen F. Bart, Rodney A. Brooks, Daniel J. Ehrlich, K. R. Udayakumar and L. Eric Cross. "Piezoelectric Micromotors for Microrobots," J. Microelectromechanical Systems **1** (1) 47-50 (1992).

APPENDIX 35

A STUDY OF $Y_1Ba_2Cu_3O_{7-x}$ THICK FILMS ON FERROELECTRIC SUBSTRATES

A. Srivastava, A. Bhalla, L. E. Cross
Materials Research Laboratory
The Pennsylvania State University
University Park, PA 16802, USA.

Abstract

The goal of this study is to qualify the use of Yittrium Barium Copper Oxide films (the orthorhombic superconducting phase commonly refered to as '1-2-3,' hereafter termed as 'YBCO') as electrodes on ferroic materials for use in dielectric and piezoelectric devices. The substrates used were, Barium Titanate (BT), Lead Zirconate Titanate (PZT) and Lead Magnesium Niobate-Lead Titanate (92.5PMN-7.5PT). The YBCO films were synthesized on the substrates by spin coating, spraying, screen-printing and tape cast laminations. The dielectric loss data as a function of temperature and frequency of YBCO electroded samples indicate differing degrees of interfacial interaction. The coatings did not have a good adhesion on PMN-7.5PT. The interaction with BT was excessive. The PZT-YBCO system appears to be the most compatible with minimum adverse interactions and excellent adhesion properties without substantial loss of electrical properties.

Introduction

The three substrate materials BT, PMN-PT[1],PZT chosen for this study are the most widely used for dielectric and piezoelectric device applications. Most of these devices incorporate the use of expensive noble metals for electrodes. Even though the industry has moved away from using expensive gold-platinum electrode systems, to using less expensive silver palladium electrodes, this alternate electrode system still tends to be quite expensive. The silver-palladium electrodes (a 70:30 composition) in multilayered devices account for as much as 90% of the total material costs and 35% of the total cost of the multilayered device[2]. In addition, with silver in the electrode at the high firing temperatures (>1000°C) there is a tendency for the silver to migrate, eventually leading to failure[3].

Ni appeared to be a candidate in the late 1970's, in the US, but was not used as it was too difficult to control its properties and reliability.Also if Ni is used as a cofired electrode material, a reducing atmosphere is essential to avoid oxidation of the electrode.Hence this procedure is useless for PZT, PMN and PMN-PT compositions, as they would not densify and would have higher conductivities when sintered under reducing atmospheres.

Another problem with these metal electrodes is that the metal-ceramic interface is a site for delamination and hence causes reduced mechanical reliability. In multilayered actuators the stress concentration at the internal metal-electrode ends are considered to be the cause for failure.The main disadvantage is the mechanical britleness of these internal electrodes[4].

These electrode related problems,among others, have been the driving force towards the search for newer materials to replace the existing expensive noble metal electrodes.Certain ceramic oxides can readily cater to the specifications needed to qualify as electrodes, for the above stated applications.A large part of these highly conductive oxides belong to the Perovskite family, showing metallic behaviour and are relatively inexpensive and easy to synthesize. One such oxide, $Y_1Ba_2Cu_3O_{7-x}$ (x ranging from 0 to 0.5), having a defect Perovskite structure and lying at the semiconductor-insulator boundary will be the focus of this study, to be tested as an alternate electrode for ferroelectric devices.

The concept of using oxide electrodes was first suggested by Ashida[5] *et al* and was a theoretical report in 1968. The first practical study was done by Abe[6]*et al* where they laminated Barium Titanate with internal electrodes of La (0.15 at%) doped Barium Titanate,and cofired at 1270°C.Gaucher of Thomson-CSF, in France worked on $LaNiO_3$ as a cofired electrode material for their own proprietary dielectric compositions[7].Skeele *et al*[8] worked on using "Barium meta Plumbate as a ceramic electrode for ceramic capacitors." Nagaraj *et al*[9]did a study of YBCO high temperature superconducting electrodes for Barium Titanate ceramic capacitors.

In this study the main objective is to qualify YBCO as an electrode material. Hence more specifically to make an electrode system from commercial grade YBCO on commercial grade substrates.Test the effect of this electrode (or interfacial reaction) on the properties of the device. Based on this study a YBCO-substrate(s) combination can be selected as the main focus for an indepth study.

Experimental Work

The materials chosen for this study are listed in table I. The substrates were made by the conventional oxide mix method using 4 wt% Dupont B5200 binder with Acetone or Polyvinyl Alcohol and Glycerine. The circular pellets were pressed at 5000 psi. The firing temperatures are stated in Table I.All the samples were sintered at a slow ramp rate (~2.5°C/min) with soak times ranging from 30 minutes to 2 hours.

YBCO Coatings

The YBCO powder was coated on the sintered substrate discs by three techniques. A compressed air spray gun setup to spray a suspension of YBCO in acetone, spin coating and screen printing.Screen printing was found to be the most reliable method to lay consistent uniform coatings. The screen printing paste was made by roll milling, (in a three roll mill), YBCO with a proprietary vehicle VS633 supplied by Heraus Inc. (Union Hill Industrial Park, West Conshocken, PA 19428).

For the cofired samples the PMN-7.5PT and YBCO were tape cast seperately and then laminated at about 70°C in a laminating press.

Table I. The materials chosen for this study, their suppliers and their sintering temperatures.

Material	Sintering Temp.°C	Supplier
$BaTiO_3$	1320	TAM Ceramics Inc. Niagara Falls, NY.
PMN-7.5PT	1240	Edo Corporation, Salt Lake City, Utah.
PMN-7.5PT + Lithium Nitrate	850	Materials Research Lab., University Park, PA.
PZT	1280	Channel Products Inc., Chesterland, Ohio.
YBCO	~900	Rhone Poulenc New Jersy.

Results and Discussion

The dielectric constant and dielectric loss as a function of temperature and frequency were used to do a preliminary qualification on the compatibility of YBCO with a particular substrate. Polished substrates with sputtered gold electrodes were used as standards respectively for each YBCO-substrate system.

YBCO on Barium Titanate (BT)

The YBCO thick film coatings on BT fired in a flowing oxygen furnace, at temperatures greater than 975°C were green, insulating and had completely reacted with the substrate. Coatings fired at temperatures lower than 975°C were black and having the conductive orthorhombic phase with a room temperature resistivity of ~200 milli ohm-cm. But even in these samples the region at the interface was found to be hygroscopic and would swell causing delamination of the electrode from the substrate. Scrapings of this interacted interfacial layer could not be identified from its XRD pattern. It is suspected that this interfacial phase could be Ba_2TiO_4.It is well documented that Ba_2TiO_4 and $BaTi_3O_7$-Ba_2TiO_4 occur in poorly mixed/sintered $BaTiO_3$.This phase is characteristic for being hygroscopic and decomposes with swelling in even slightly moist air[11]. $BaTiO_3$ with this phase may show excellent dielectric and piezoelectric properties but with time the dielectric loss rises to an unstable magnitude.

A previous study of YBCO thin films grown on (001) $BaTiO_3$ single crystals by Li *et al*[11] reported strong interactions of these films with the single crystal substrate.The X-ray patterns of these films (35 um) had an additional peak (d=2.11 A) which they tentatively attributed to $Ba_2Ti_5O_{12}$, an interface reaction compound. To understand this interaction between YBCO and BT a study of intermixed solid solutions is being conducted, the results of which will be published in the near future. In order to see the performance of YBCO as a physically bonded electrode, YBCO sintered discs (950°C, 2 hours in O_2) were bonded onto the opposite sides of a BT sintered disc with silver paste at the YBCO-BT interfaces.The dielectric loss data as a function of temperature and frequency, compared to gold electroded BT are shown in figures 1a through d.From this data it appears that if the interfacial reaction in fired samples can be minimised by a barrier layer YBCO may still have potential as an oxide electrode on BT.

YBCO on PMN-7.5PT

The YBCO coatings on sintered PMN-7.5PT were fired at temperatures between 900 to 975°C. There was inadequate bonding of YBCO on PMN-7.5PT. Hence similar to BT, physically sandwiched YBCO electrodes were used on sintered PMN-7.5PT discs, and their dielectric constant and loss response was compared to gold electroded PMN-7.5PT.The data is presented in figures 2 a through d. The physically bonded electrodes,as in the case with BT, show a response identical to gold electroded samples.

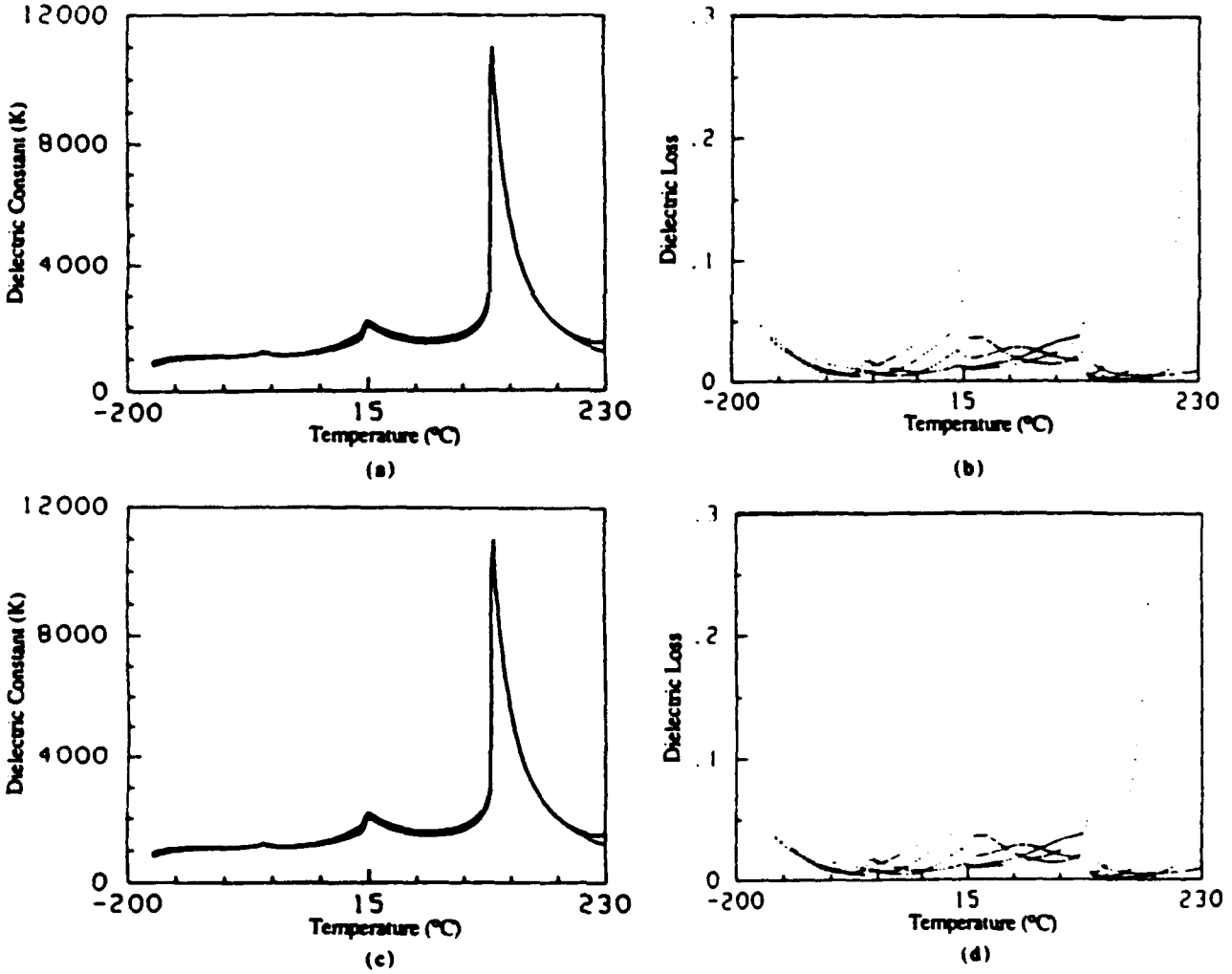

Figure 1. The dielectric constant and the loss as a function of temperature at four frequencies,100Hz, 1000Hz, 10,000Hz and 100,000Hz. Figure 1(a) and (b) are for BT with sputtered gold on polished surfaces, (c) and (d) are for YBCO-BT samples physically bonded with silver paste.

Cofired YBCO on PMN-7.5PT. The sintering temperature of PMN-7.5PT was reduced to 850°C by addition of 2 mol% $LiNO_3$. This enabled us to cofire the laminated tape cast sheets of YBCO and the fluxed PMN-7.5PT. The dielectric response is shown in figures 3 a through d. We see that there is a greater frequency dependence for the YBCO electroded samples and a decrease in the dielectric constant. The dielectric loss data indicates very large losses at the transition temperature and an increase in losses with temperature. This may be attributed to diffusion of lithium ions into the interface and possibly the electrode itself. $LiNO_3$ decomposes at 600°C and is a fugitive phase. Hence a sintering study with microstructral characterization would be necessary to enable a clean and complete removal of lithium from this system.

YBCO on PZT

YBCO readily adheres onto PZT at 950°C, one hour soak. At first this seemed surprising as YBCO did not adhere to PMN-7.5PT very well, and since PZT requires a higher sintering temperature, no adhesion was expected. TGA (Thermal Gravimetric Analysis) comparing the two powders, figure 4, indicated that the vapour pressure of PbO in PMN-7.5PT is different than that of PZT. PbO leaves the PZT structure at a lower temperature and at a much faster rate than it does in PMN-7.5PT. We infer from this data that PbO is essential for adhesion of YBCO to lead based substrates.

The dielectric response of YBCO electroded PZT is shown in figures 5 a through d. We do not see a decrease in the dielectric constant as a function of temperature, when compared to the standard, but there is a slight frequency dependence which increases with temperature. The losses increase with temperature due to increased conduction. But in the vicinity of room temperature the properties are comparable to the gold electroded samples.

Conclusions

The YBCO material is a semiconductor at room temperature with metallic behaviour. It was found to react excessively with BT. An interfacial layer, probably Barium rich is formed in all cases and was hygroscopic in nature. The YBCO electrode did not adhere onto PMN-7.5PT with any reliable mechanical integrity. PbO seems to play a key role for adhesion in these lead based compositions. The PMN-7.5PT compositions coated with YBCO and cofired showed excessive losses and lower dielectric constants possibly due to lithium interaction at the interface. From this preliminary study we observe that YBCO has maximum potential as an electrode on PZT compositions.

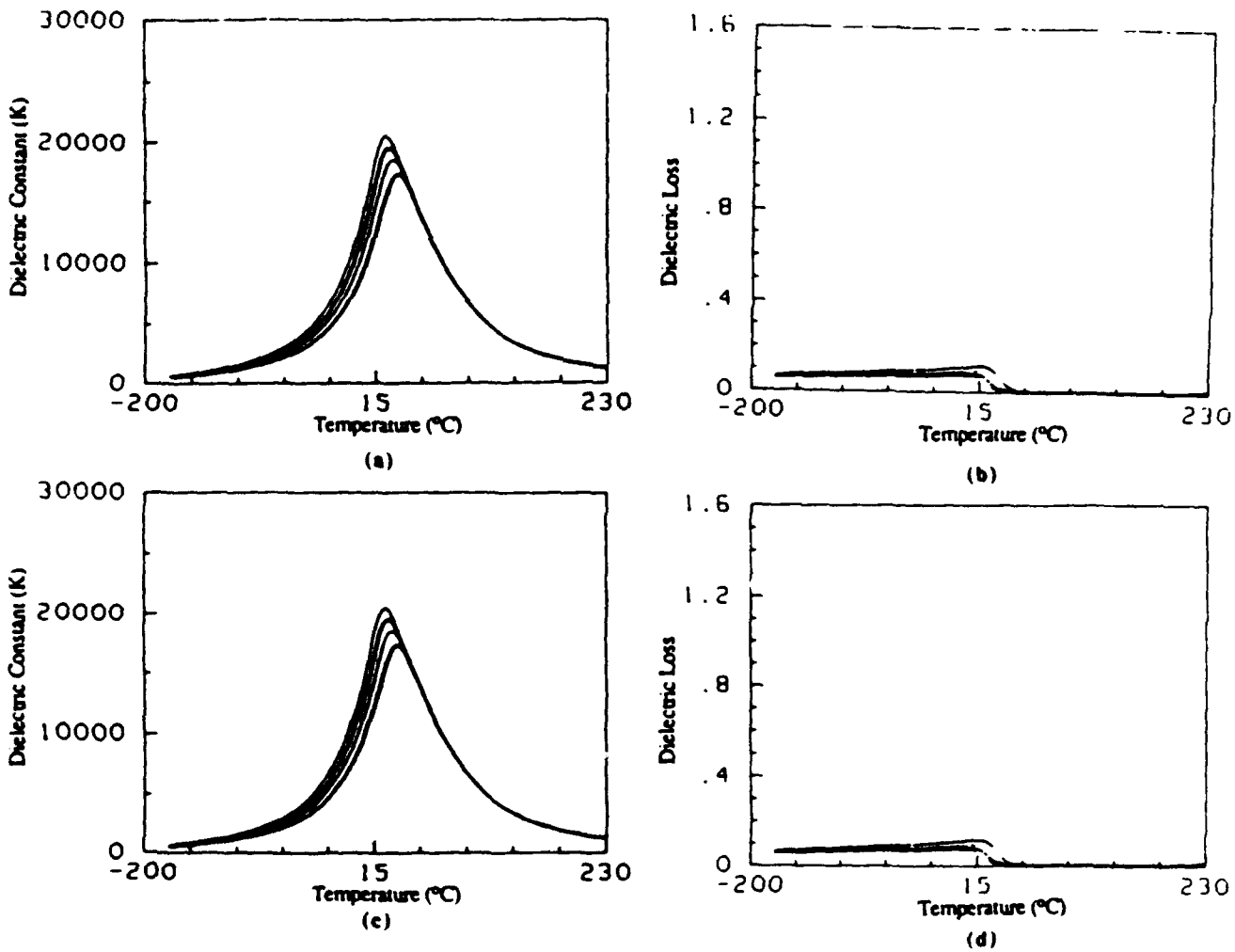

Figure 2. The dielectric constant and the loss as a function of temperature at four frequencies, 100Hz, 1000Hz, 10,000Hz and 100,000Hz. Figure 2 (a) and (b) are for PMN-7.5PT with sputtered gold on polished surfaces, (c) and (d) are for YBCO/PMN-7.5PT samples physically bonded with silver paste.

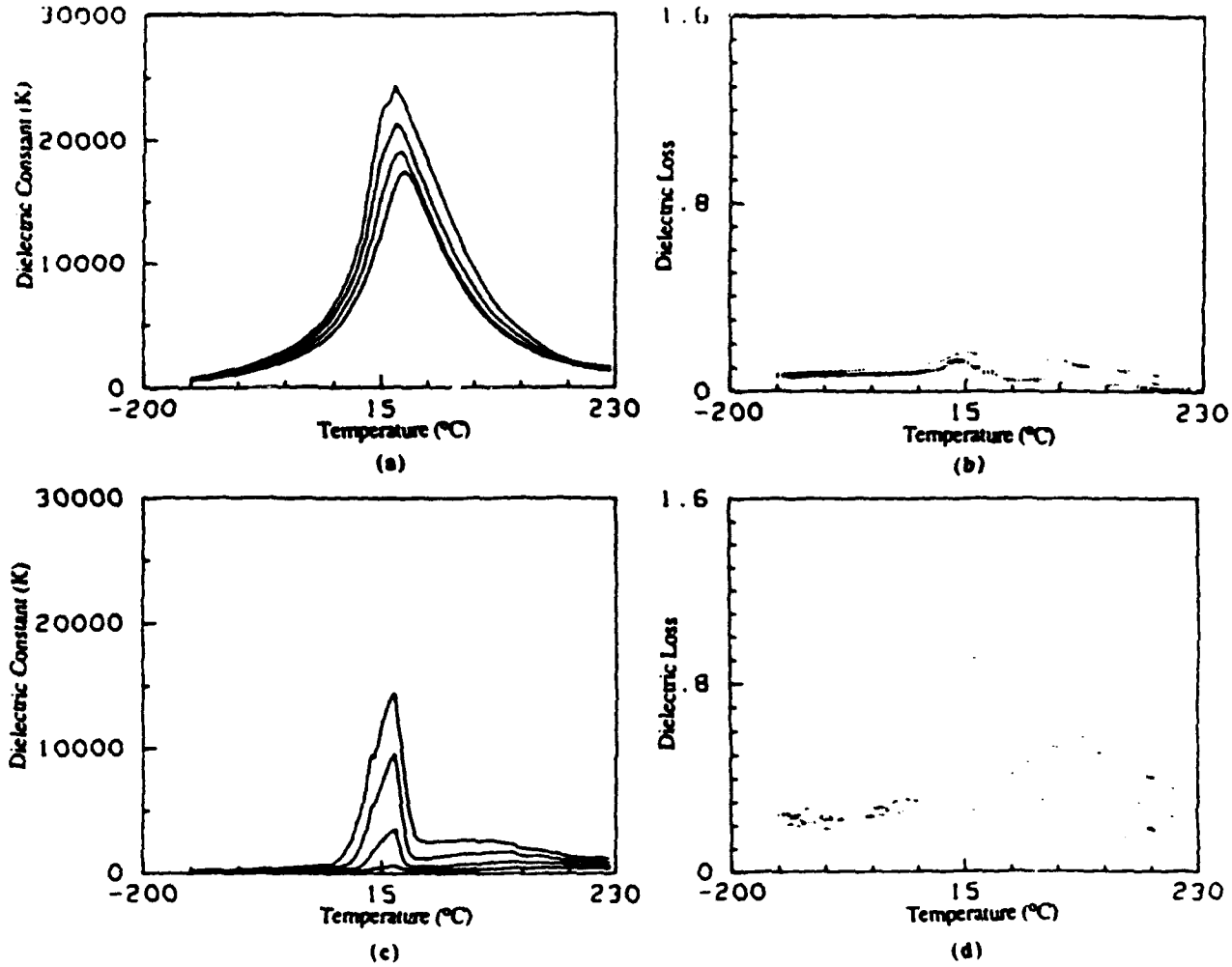

Figure 3. The dielectric constant and the loss as a function of temperature at four frequencies, 100Hz, 1000Hz, 10,000Hz, 100,000Hz. Figures 1 (a) and (b) are for PMN-7.5PT + Lithium Nitrate with sputtered gold on polished surfaces, (c) and (d) are for YBCO laminated on (PMN-7.5PT + Lithium Nitrate) samples, cofired at 850°C.

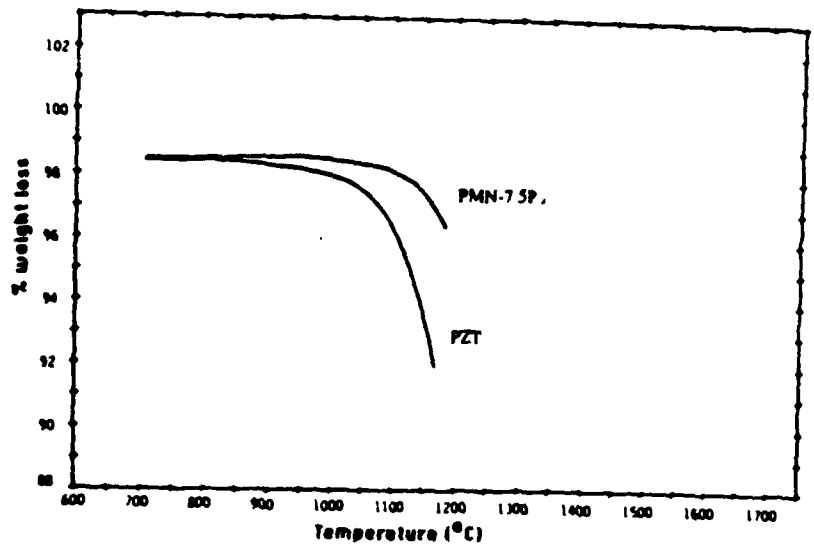

Figure 4. A comparitive Thermal Gravimetric Analysis (TGA) of PZT and PMN-7.5PT. The decrease in weight is from PbO leaving the system. PbO volatizes from PZT earlier and more rapidly than in PMN-7.5PT.

References

[1] T.R. Shrout and J.P. Dougherty, "A world review on lead based $Pb(B_1B_2)O_3$ relaxors vs $BaTiO_3$ dielectrics for multilayer capacitors." Ceramic Transactions, Vol. 8, Eds. H. C. Ling and M. F.. Yan, pp. 3-19 (1990).

[2] Technological and Economical Assessment of Advanced Ceramic Materials, Volume 3."A case study of ceramic capacitors" prepared by Charles River Associates Incorporated for the National Bureau of Standards, U.S. Department of Commerce, August 1984. p252, Advanced Ceramic Materials, Noyes Publication,Park Ridge,New Jersy,U.S.A.

[3] H.C.Ling and A.M.Jackson,"Correlation of Silver Migration with Temperature-Humidity- Bias (THB) Failures of Multilayer Ceramic Capacitors," IEEE Trans. Comp.,Hybrids, and Manuf. Tech., 12, pp130-133 (1989).

[4] S.Takahashi, Ceramic Bulletin, 1986, Vol. 65, No. 8, pp1156 - 1157.

[5] T. Ashide, K. Sawamoto and H. Toyoda, *Kenkyu Jitsuyoka Houkoku*, 17-2,365 (1968) - as quoted in reference [6].

[6] K. Abe, K. Uchino and the late S. Nomura, Ferroelectrics, 1986, Vol. 68, pp215-223.

[7] P. Gaucher, Thomson-csf, Orsay Cedex, France.As quoted in reference [8].

[8] F.P. Skeele, An investigation using Barium meta Plumbate as a ceramic electrode for ceramic capacitors., August 1985, M.S. Thesis in Ceramic Science, The Pennsylvania State University, University Park, PA 16802, USA.

[9] Raviprakash Nagaraj, Investigation of Yittrium Barium Copper Oxide High Temperature Superconducting Electrodes for Barium Titanate Ceramic Capacitors,1990, M.S. Thesis, The Pennsylvania State University, University Park,PA 16802.

[10] B. Jaffe, W.R. Cook Jr. and H. Jaffe: Piezoelectric Ceramics, 1971, p62.

[11] Z.Z. Li, A. Perrin, J. Padiou, M. Sergent and J. Godard, Materials Letters Vol.7, No. 5,6 Nov. 1988 pp178-181.

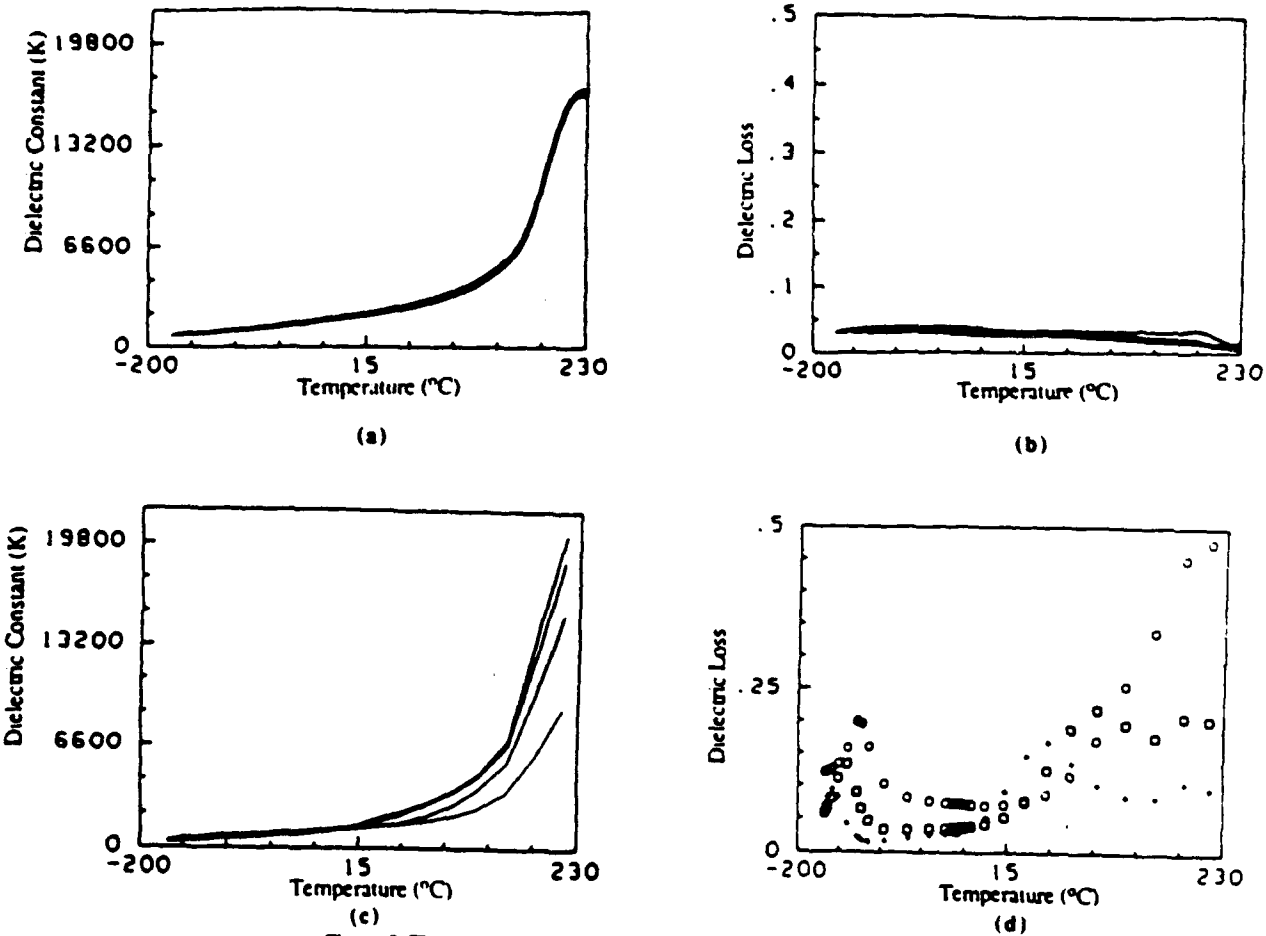

Figure 5. The dielectric constant and the loss as a function of temperature at four frequencies.100Hz, 1000Hz, 10,000Hz and 100,000Hz. Figure 5(a) and (b) are for PZT samples with sputtered gold on polished surfaces, (c) and (d) are for YBCO electroded on PZT, sintered at 950°C, 1 hour.

APPENDIX 36

Ferroelectrics, 1991, Vol. 123, pp. 243–251
Reprints available directly from the publisher
Photocopying permitted by license only

$Y_1Ba_2Cu_3O_{7-x}$ AS AN ELECTRODE MATERIAL FOR FERROELECTRIC DEVICES

A. SRIVASTAVA, A. BHALLA, and L. E. CROSS
Materials Research Laboratory, The Pennsylvania State University, University Park, PA 16802, USA

(Received October 12, 1991)

$Y_1Ba_2Cu_3O_{7-x}$ (YBCO) was studied as a potential electrode material for devices utilizing perovskite ferroelectric materials. Electrode thick film coatings were made on Barium Titanate (BT), Lead Magnesium Niobate-Lead Zinc Niobate (PMN-24 PZN), Lead Magnesium Niobate-Lead Titanate (PMN-7.5PT) and Lead Zirconate Titanate (PZT). Conventional slow fire techniques with flowing oxygen were initially used to fire the electrode onto the substrate. These 24 hour firing cycles caused excessive interactions at the electrode-substrate interface, as determined by dielectric constant and loss data. PbO vapor pressure was found to play a key role in the adhesion of these coatings.

An alternate "fast fire" technique was excellent in producing conductive, adhering electrode coatings. YBCO electroded PZT samples performed identical to PZT electroded with gold. The YBCO electrode was found to react more with the PMN based substrates.

Keywords: oxide electrode, dielectric constant, dielectric loss, thick film, perovskite

INTRODUCTION

$Y_1Ba_2Cu_3O_{7-x}$ (YBCO) is a "high" temperature superconductor with an approximate room temperature conductivity of ~1 milli ohm-cm (for commercial grade powders). The crystal structure of YBCO is a defect perovskite with sintering temperatures around 900°–975°C, in ambient or oxidising atmospheres. Based on these properties it was considered that this oxide has a potential as a non-conventional electrode for use in many of the widely used perovskite ferroelectrics.

In the present electronics market the materials most widely used for dielectric, piezoelectric and electrostrictive applications are Barium Titanate, Lead Zirconate Titanate and Lead Magnesium Niobate solid solutions with Lead Titanate or Lead Zinc Niobate.[1] These devices incorporate the use of expensive noble metals for electrodes. The industry has moved away from using expensive gold-platinum electrode systems to less expensive silver palladium electrodes, this alternate electrode system still tends to be quite expensive. The silver-palladium electrodes (a 70:30 composition) in multilayered devices account for as much as 90% of the total material costs and about 35% of the total cost of the multilayered device.[2]

Ni appeared to be a candidate in the late 1970's, in the US, but was not used as it was too difficult to control its properties and reliability. Also if Ni is used as a cofired electrode material, a reducing atmosphere is essential to avoid oxidation of the electrode. Hence nickel, copper and other base metals are useless for PZT, PMN and PMN-PT compositions, as they would not densify and would have higher conductivities when sintered under reducing atmospheres. Another problem with these metal electrodes is that the metal-ceramic interface is a site for delamination

and hence causes reduced mechanical reliability. In multilayered actuators the stress concentration at the internal metal-electrode ends are considered to be the cause for failure. The main disadvantage is the mechanical brittleness of these internal electrodes.[3]

The above stated disadvantages in conventional electrodes have been the driving force towards the search for alternate materials to replace the presently used expensive noble metal electrodes. Certain ceramic oxides can readily cater to the specifications needed to qualify as electrodes for the above stated applications. A large part of these highly conductive oxides belong to the perovskite family. They show metallic behavior, are relatively inexpensive and some require oxidising atmospheres during sintering. One such oxide, $Y_1Ba_2Cu_3O_{7-x}$ (x ranging from 0 to 0.5), having a defect perovskite structure and lying at the semiconductor-insulator boundary will be the focus of this study to be tested as an alternate electrode for ferroelectric devices.

The concept of using oxide electrodes was first suggested by Ashida *et al.*[4] and was a theoretical report in 1968. The first practical study was done by Abe *et al.*[5] where they laminated Barium Titanate with internal electrodes of La (0.15 at %) doped Barium Titanate, and cofired at 1270°C. Gaucher of Thomson-CSF, in France worked on $LaNiO_3$ as a cofired electrode material for their own proprietary dielectric compositions.[6] Skeele *et al.*[7] worked on using "Barium meta Plumbate as a ceramic electrode for ceramic capacitors."

In this study the main objective was to qualify YBCO as an electrode material. Hence more specifically to make an electrode system from commercial grade YBCO on commercial grade polycrystalline subtrates. The YBCO electroded samples were tested and characterized for the effects of the interfacial reaction on the electrical properties of the device.

EXPERIMENTAL WORK

The materials chosen for this study are listed in Table I. The substrates were made by the conventional oxide mix method using 4 wt% Dupont B5200 binder with Acetone or a water based binder with Polyvinyl Alcohol and Glycerine. The circular pellets were pressed at 5000 psi. The firing temperatures are stated in Table I. All the samples were sintered at a slow ramp rate (~2.5°C/min) with soak times ranging from 30 minutes to 2 hours.

TABLE I

The materials chosen for this study, their suppliers and their sintering temperatures

Material	Sintering Temp.°C	Supplier
$BaTiO_3$	1320	TAM Ceramics Inc. Niagara Falls, NY.
PMN-7.5PT	1240	Edo Corporation, Salt Lake City, Utah.
PMN-24PZN	1140	Materials Research Lab., University Park, PA.
PZT	1280	Channel Products Inc., Chesterland, Ohio.
YBCO	~900	Rhone Poulerc New Jersy.

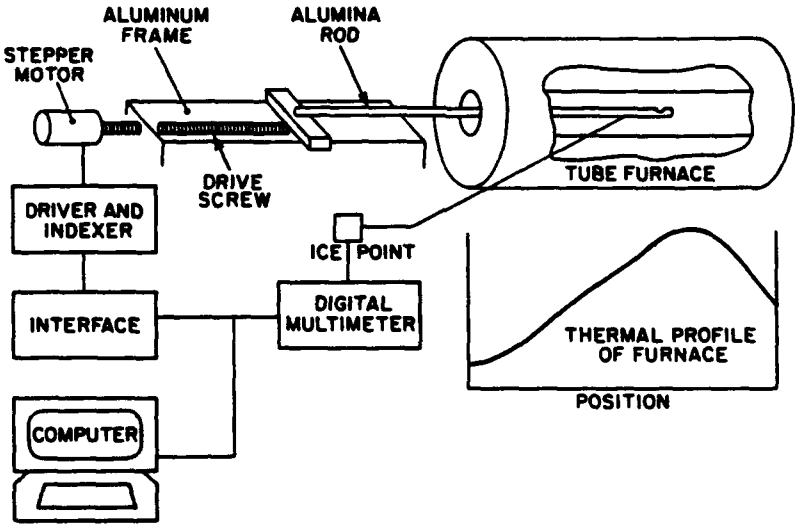

FIGURE 1 A flow chart of the setup used for fast firing.

YBCO Coatings

The YBCO powder was coated on the sintered substrate discs by three techniques. A compressed air spray gun setup to spray a suspension of YBCO in acetone, spin coating and screen printing. Screen printing was found to be the most reliable method to lay consistent uniform coatings. The screen printing paste was made by roll milling, (in a three roll mill), YBCO with a proprietary vehicle VS633.†

Sintering the Electrode onto the Substrate

The YBCO coated samples were fired using two techniques. Slow firing in a mullite tube furnace in flowing oxygen, due to the intercalating properties of YBCO. Another technique used was a fast firing technique. Figure 1 is a flow-chart of the set-up used for fast firing. The rapid thermal profiles were obtained through the use of specially designed, computer automated, furnace and driver system. The tube furnace was heated to an equilibrium set point temperature. The temperature was then measured as a function of distance into the furnace. The thermal profile was subsequently stored in the memory of a Hewlett-Packard HP9816 computer. A detailed description of this system has been published elsewhere.[8,9]. Figures 2(a) and (b) compare the firing schedules used in the conventional and the fast fire techniques.

RESULTS AND DISCUSSION

The dielectric constant and dielectric loss as a function of temperature and frequency were used to qualify the compatibility of YBCO with a particular substrate.

†Heraus Inc. Union Hill Industrial Park, West Conshocken, PA 19428.

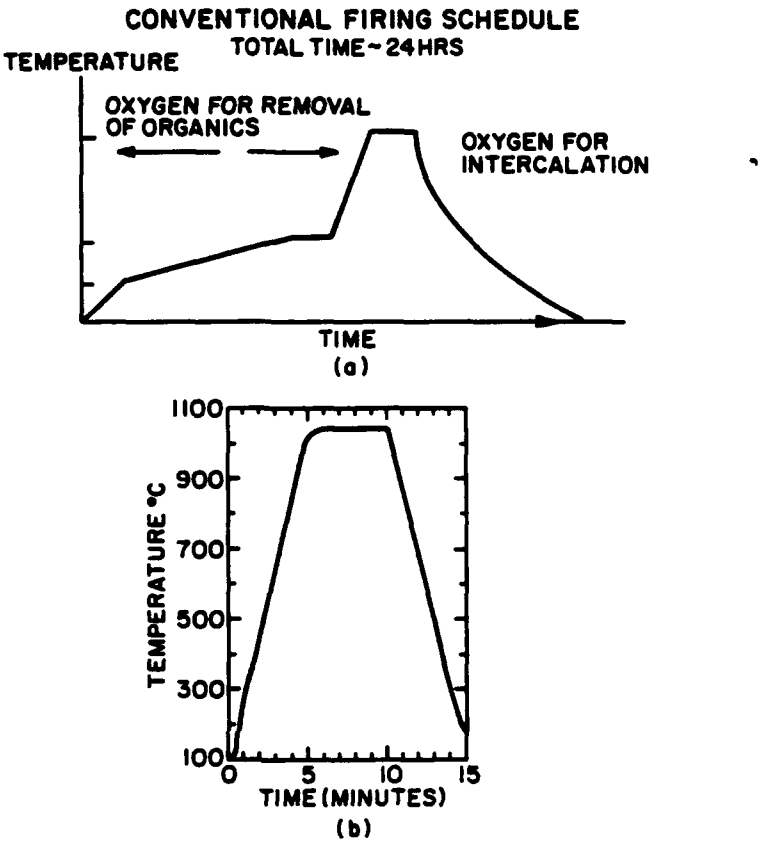

FIGURE 2(a) and (b) Compare the firing schedules used in the conventional tube furnaces with the fast fire setup.

Polished substrates with sputtered gold electrodes were used as standards respectively for each YBCO-substrate system.

CONVENTIONAL SLOW FIRING OF YBCO COATED SAMPLES

YBCO on Barium Titanate (BT)

The YBCO thick film coating on BT fired in a flowing oxygen furnace, at temperatures greater than 975°C were a green phase, highly insulating and had completely reacted with the substrate. Coatings fired at temperatures lower than 975°C were black and have the conductive orthorhombic phase with a room temperature resistivity of ~200 milli ohm-cm. But even in these samples the region at the interface was found to be hygroscopic and would swell causing delamination of the electrode from the substrate. Scrapings of this interacted interfacial layer could not be identified from its XRD pattern. It is suspected that this interfacial phase could be Ba_2TiO_4. It is well documented that Ba_2TiO_4 and $BaTi_3O_7.Ba_2TiO_4$ occur in

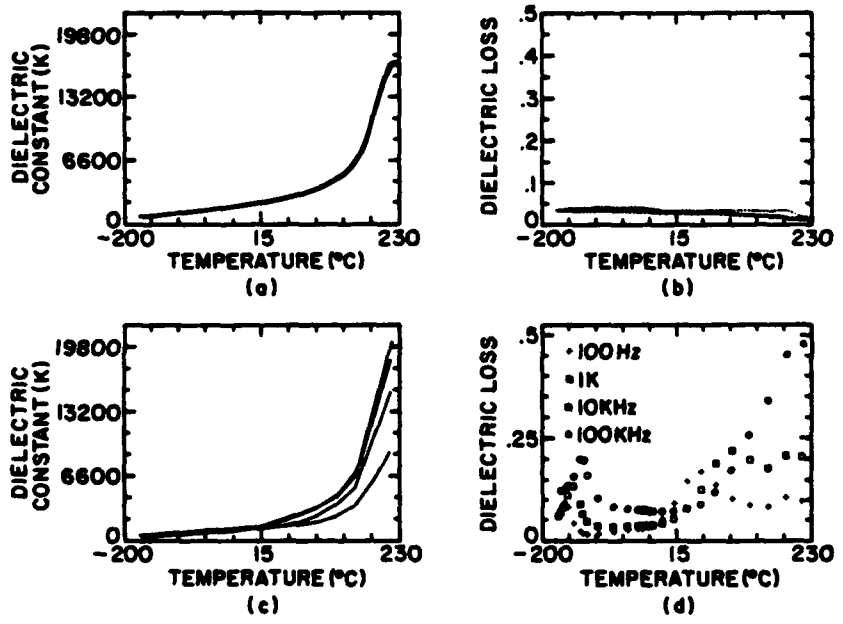

FIGURE 3(a) through (d) The dielectric constant and loss as a function of temperature at four frequencies, 100 Hz, 1000 Hz, 10000 Hz, and 100000 Hz. The (a) and (b) are for samples electroded with sputtered gold on polished surfaces, (c) and (d) are for YBCO electroded on PZT, sintered at 950°C, 1 hour.

poorly mixed/sintered $BaTiO_3$. This phase is characteristic for being hygroscopic and decomposes with swelling in even slightly moist air.[10] $BaTiO_3$ containing this phase may show excellent dielectric and piezoelectric properties but with time the dielectric loss rises to an unstable magnitude.

A previous study of YBCO thin films grown on (001) $BaTiO_3$ single crystals by Li *et al.*[11] reported strong interactions of these films with the single crystal substrate. The X-ray patterns of these films (35 μm) had an additional peak ($d = 2.11\ A$) which they tentatively attributed to $Ba_2Ti_5O_{12}$, an interface reaction compound. To understand this interaction between YBCO and BT a study of intermixed solid solutions is being conducted, the results of which will be published in the near future. In order to see the performance of YBCO as a physically bonded electrode, YBCO sintered discs (950°C, 2 hours in O_2) were bonded onto the opposite sides of a BT sintered disc with silver paste at the YBCO-BT interfaces. The dielectric loss data as a function of temperature and frequency of these samples compared to gold electroded BT were identical. From this data it appears that if the interfacial reaction in fired samples can be minimized YBCO may still have potential as an oxide electrode on BT.

YBCO on PMN-7.5PT

The YBCO coatings on sintered PMN-7.5PT were fired at temperatures between 900–975°C. There was inadequate bonding of YBCO on PMN-7.5PT. Hence similar to BT, physically sandwiched YBCO electrodes were used on sintered PMN-

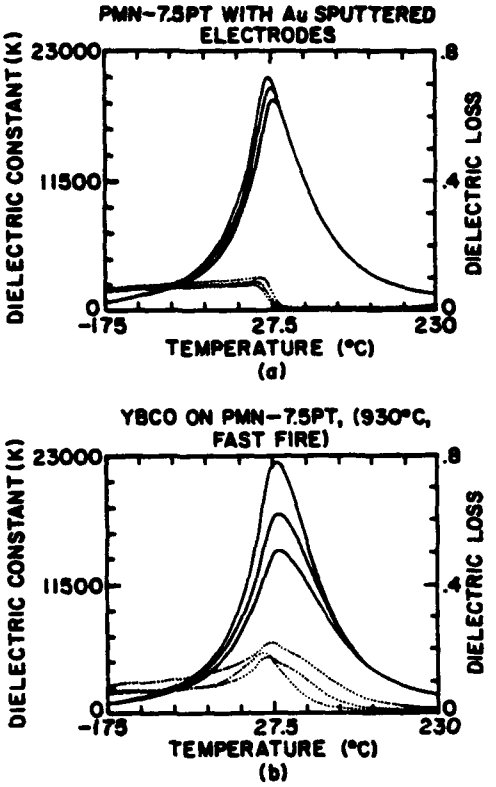

FIGURE 4(a) and (b) A comparison of the dielectric response of PMN-7.5PT electroded with gold and YBCO electrodes, at three different frequencies, 100 Hz, 1000 Hz, 10000 Hz.

7.5PT discs, and their dielectric constant and loss response was compared to gold electroded PMN-7.5PT. The physically bonded electrodes, as in the case with BT, show a response identical to gold electroded samples.

YBCO on PZT

YBCO readily adheres onto PZT at 950°C, one hour soak. The comparative dielectric response of YBCO electroded PZT is shown in Figures 3a through d. We observe the effects of the interaction causing a frequency dependence in the dielectric constant and increased losses especially at higher temperatures. Around room temperature the dielectric constant and losses were comparable to the gold standard samples. This indicated that though an adverse interfacial layer was forming the YBCO-PZT system had the maximum potential.

Fast Firing of YBCO Coated Substrates

Based on results of slow firing it was hoped to reduce the interaction at the interface using a rapid 15 minute firing cycle. As shown below this technique, even on

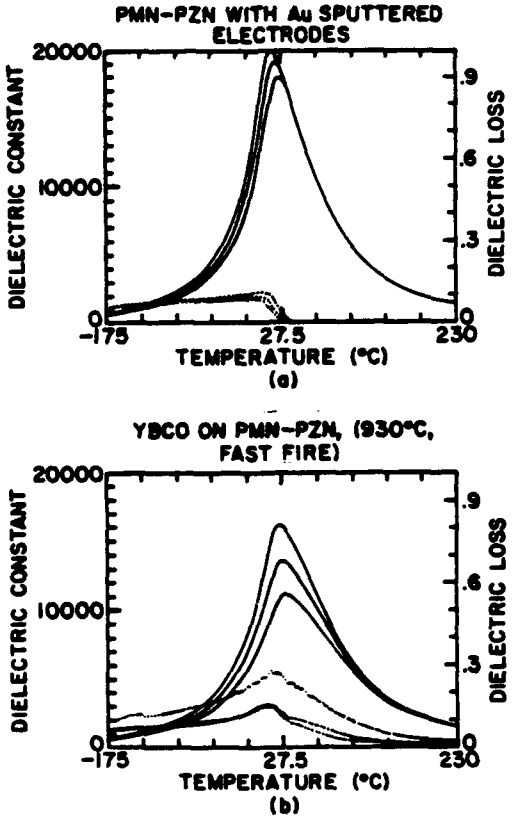

FIGURE 5(a) and (b) A comparison of the dielectric response of PMN-24PZN electroded with gold and YBCO electrodes, at three different frequencies, 100 Hz, 1000 Hz, 10 000 Hz.

preliminary attempts, was most successful in reducing the interactions resulting in improved adhesion and excellent dielectric properties. For this study all fast fired samples were sintered under similar firing schedules and conditions.

YBCO on PMN-7.5PT

The YBCO coatings on PMN-7.5PT had excellent adhesion, fast fired at 930°C with a rise time of 5 minutes, a soak time of 5 minutes and a cooling time of 5 minutes. On analyzing the dielectric data, Figures 4(a) and (b), we observe a decrease in the dielectric constant with increasing frequency and the presence of a lossy interfacial layer.

YBCO on PMN-24 PZN

This composition like the PMN-7.5PT was chosen for its dielectric constant maxima occurring at room temperature. The YBCO had excellent adhesion properties but

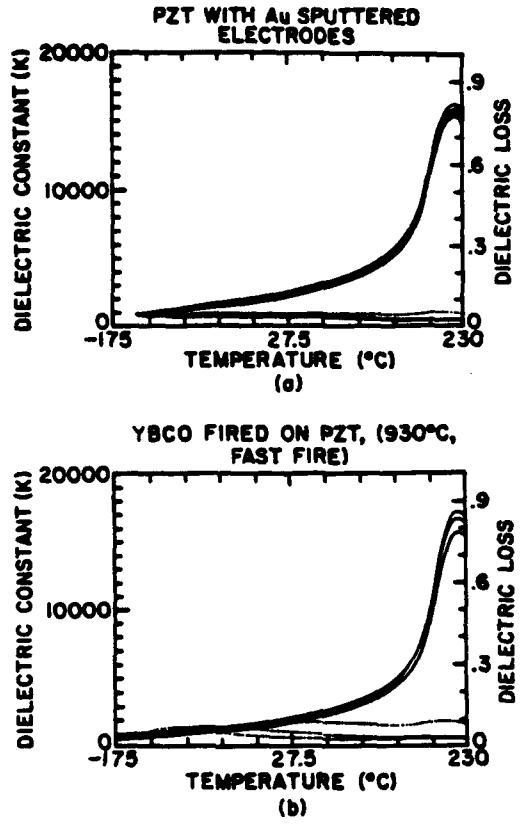

FIGURE 6(a) and (b) A comparison of the dielectric response of PZT electroded with gold and YBCO electrodes, at three different frequencies, 100 Hz, 1000 Hz and 10 000 Hz.

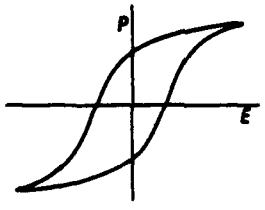

FIGURE 7 A hysteresis loop of PZT electroded with YBCO, under a 50 HZ sinusoidal electric field, showing good ferroelectric behavior with no conduction effects or other deterioration induced due to the YBCO electrode.

the YBCO coated samples showed a dielectric response similar to the PMN-7.5PT samples as shown in Figures 5(a) and (b).

YBCO Coated on PZT

YBCO on PZT had both excellent adhesion properties and dielectric response.

The dielectric constant and losses were almost identical to the gold standard. The dielectric responses are compared in Figures 6(a) and (b). The hysteresis behavior of YBCO electroded PZT is clearly ferroelectric, Figure 7 shows the typical ferroelectric hysteresis loop.

CONCLUSIONS

We have demonstrated that YBCO can be used as an electrode. It was found to react excessively with BT. An interfacial layer, probably barium rich is formed which is hygroscopic in nature. The YBCO electrode did not adhere onto PMN-7.5PT with any reliable mechanical integrity when fired using the slow firing technique. PbO seems to play a key role for adhesion in these lead based compositions, the PbO vapor pressure in the PMN systems is higher than in PZT causing an earlier and more rapid loss of PbO (this was determined on comparing the thermal gravimetric analysis of PMN-7.5PT with PZT). The interfacial interactions were drastically reduced using a fast firing technique. The adhesion characteristics were greatly improved. The fast firing schedule was not varied for the different substrate systems. The 930°C/5 minute soak proved to be excellent for the PZT substrates. The PMN system appears to be more reactive with YBCO and hence a more detailed firing study is being conducted to optimize this system. The PZT samples electroded with YBCO showed a typical ferroelectric hysteresis loop with the coercive field being 16 kilo V/cm. The PZT samples electroded with YBCO had a dielectric response identical to PZT electroded with gold.

REFERENCES

1. T. R. Shrout and J. P. Dougherty, "A world review on lead based $Pb(B_1B_2)O_3$ relaxors vs $BaTiO_3$ dielectrics for multilayer capacitors." *Ceramic Transactions*, **8**, Eds. H. C. Ling and M. F. Yan, pp. 3–19 (1990).
2. Technological and Economical Assessment of Advanced Ceramic Materials, Volume 3. "A case study of ceramic capacitors" prepared by Charles River Associates Incorporated for the National Bureau of Standards, U.S. Department of Commerce, August 1984. p. 252, *Advanced Ceramic Materials*, Noyes Publication, Park Ridge, New Jersey, U.S.A.
3. S. Takahashi, *Ceramic Bulletin*, **65**, 8, pp. 1156–1157 (1986).
4. T. Ashide, K. Sawamoto and H. Toyoda, *Kenkyu Jitsuyoka Houkoku*, 17-2,365 (1968) - as quoted in reference [6].
5. K. Abe, K. Uchino and the late S. Nomura, *Ferroelectrics*, 1986, Vol. 68, pp. 215–223.
6. P. Gaucher, Thomason-csf, Orsay Cedex, France. As quoted in reference [8].
7. F. P. Skeele, *An investigation using Barium meta Plumbate as a ceramic electrode for ceramic capacitors*, August 1985, M. S. Thesis in Ceramic Science, The Pennsylvania State University, University Park, PA 16802, U.S.A.
8. B. H. Fox, G. O. Dayton, P. Moses and J. V. Biggers, "A Controlled Temperature Profile Firing," *American Ceramic Society Bulletin*, **64**(8), pp. 141–143, 1985.
9. B. H. Fox, B. O. Dayton and J. V. Biggers, "Controlled Temperature Profile Firing System," in Annual Report of Industry/National Science Foundation Center for Dielectric Studies, by J. V. Biggers, Center Director (May 1985).
10. B. Jaffe, W. R. Cook Jr. and H. Jaffe: *Piezoelectric Ceramics*, 1971, p. 62.
11. Z. Z. Li, A. Perrin, J. Padiou, M. Sergent and J. Godard, *Materials Letters*, 7, No. 5, 6 Nov. 1988, pp. 178–181.

FERROELECTRIC THIN FILMS

APPENDIX 37

Polarization reversal and high dielectric permittivity in lead magnesium niobate titanate thin films

K. R. Udayakumar, J. Chen, P. J. Schuele,[a] L. E. Cross, V. Kumar, and S. B. Krupanidhi
Materials Research Laboratory, The Pennsylvania State University, University Park, Pennsylvania 16802

(Received 7 October 1991; accepted for publication 20 December 1991)

Ferroelectric thin films of the morphotropic phase boundary composition in the lead magnesium niobate-lead titanate solid solution system were fabricated through the sol-gel spin-on technique. The rapid thermally annealed films showed a very high dielectric constant of 2900, with a concomitant low dissipation factor of 0.02; the films were hysteretic with a saturation remanence of 11 $\mu C/cm^2$ and a coercive voltage of 0.5 V. The storage charge density observed at 5 V was 210 $fC/\mu m^2$. These films merit consideration for potential application in ferroelectric nonvolatile random access memories (NVRAMs), and in high bit density metal-oxide-semiconductor (MOS) dynamic random access memories (DRAMs).

Depending on the lead titanate content, the lead magnesium niobate $Pb(Mg_{0.33}Nb_{0.67})O_3$ (PMN)-lead titanate $PbTiO_3$ (PT) solid solution system embraces a range of compositions that are of paramount importance technologically. Bulk ceramic compositions close to the PMN end of the phase diagram[1] with high dielectric constants ($\epsilon_r > 30\,000$) find wide applications in the capacitor industry; compositions near the morphotropic phase boundary (with a PMN/PT mode ratio of 65/35) are of a ferroelectric hysteretic character, exhibiting high polarization and low coercive field. The intent of this study was to fabricate and characterize the latter composition in thin-film form for potential application in ferroelectric NVRAMs, and as high dielectric constant capacitors in ultralarge scale integrated (ULSI) dynamic RAMs.

As in bulk ceramics,[2] difficulties in obtaining the proper ferroelectric perovskite phase, devoid of the pyrochlore phase, underscore attempts at preparation of thin films of the lead magnesium niobate titanate family of materials through the sol-gel spin-on technique.[3] Fast firing of PMN at 800 °C[4,5] alleviated the problem to some extent, with a reported film dielectric constant of 1100[4] which is an order of magnitude lower than the bulk. In an earlier undertaking,[6] sol-gel derived thin films of the morphotropic phase boundary composition had to be furnace annealed at 700 °C for more than 2 h to eliminate the pyrochlore phase. In this letter, the structural and electrophysical properties of films that were rapid thermally annealed will be discussed.

The method of preparation of the sol was broadly analogous to that of lead zirconate titanate (PZT), described elsewhere.[7] In brief: the precursors employed for the preparation were lead acetate trihydrate, magnesium ethoxide, niobium ethoxide, and titanium isopropoxide, with 2-methoxyethanol as the solvent. Lead acetate trihydrate was dissolved in the solvent, and the water of hydration removed through a series of distillations. The moisture sensitive alkoxides were then added, and after prolonged refluxing to promote formation of the mixed, complex alkoxides,[8,9] the solution was heated until the temperature of the condensing vapor reached that of pure 2-methoxyethanol; the cooled solution was then hydrolyzed sparingly. Using this sol, the films were fabricated through a multistep spin-on procedure, with intermediate pyrolysis at 400 °C after each deposition for removal of the organics. Films were deposited on (100) silicon wafers with 0.15-μm-thick platinum electrodes sputtered on a thermally grown SiO_2 buffer layer. The films were annealed in an AG Associates Rapid Thermal Processor (Heat Pulse 210T) that can generate very high ramp rates (700 °C in 8 s).

The XRD pattern of films rapid thermally annealed at 850 °C for 30 s is shown in Fig. 1, from which it is apparent that the extremely high rate of annealing has the effect of suppressing the pyrochlore phase formation. Figure 2 represents the planar scanning electron micrographs of films 0.44-μm-thick rapid thermally annealed at 850 °C for 10 s

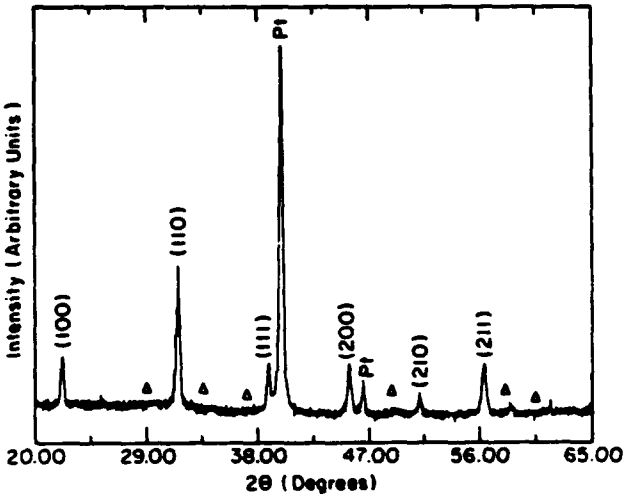

FIG. 1. XRD pattern of films rapid thermally annealed at 850 °C for 30 s. The films were grown on buffered Si, with Ti-Pt as the bottom electrode. The triangular marks correspond to the peak positions of the pyrochlore phase if it were to co-exist with the perovskite phase.

[a]Ramtron International Corporation, Colorado Springs, CO 80921.

 0003-6951/92/101187-03$03.00

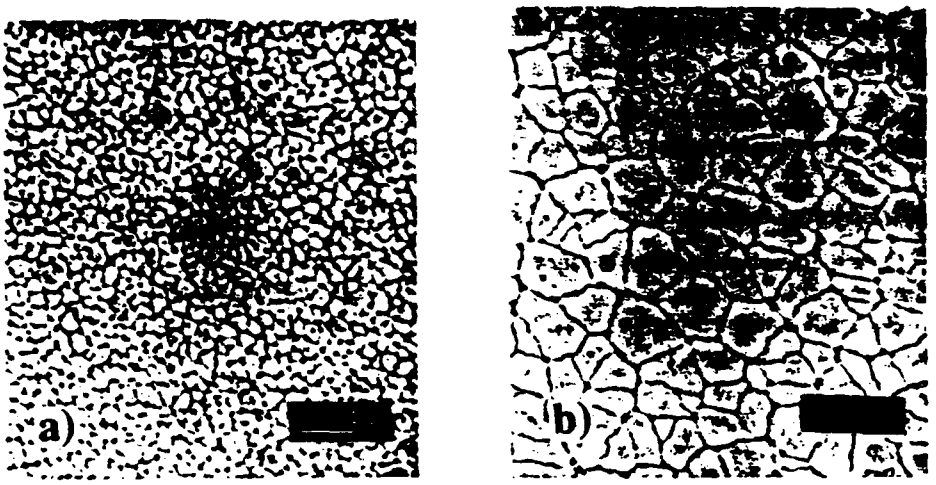

FIG. 2. Planar microstructure of rapid thermally annealed films at 850 °C for (a) 10 s and (b) 60 s. Note the dramatic increase in grain size with prolonged annealing.

and 60 s, showing a dense, equiaxed microstructure. Prolonged annealing at 60 s led to the growth of grains up to 1 μm, from approximately 0.1 μm when annealed at 850 °C for 10 s.

Using an impedance analyzer, the small-signal dielectric properties of the films were determined at room temperature, and as a function of temperature above the ambient, at frequencies below resonance. The room-temperature relative permittivity and dissipation factor at 10 kHz were 2900 and 0.02, respectively (Fig. 3), comparing favorably with the bulk ceramic of equivalent composition ($\epsilon_r = 3100$). This magnitude of dielectric permittivity is probably the highest that has been reported for any dielectric thin film in literature, be it polar or nonpolar. Thus these films are potentially useful for MOS DRAMs because the high permittivity allows a higher charge storage density so that DRAM cell size could be smaller than is possible with conventional silicon dielectric technology.

Dielectrics other than the currently prevalent SiO_2 and Si_3N_4-SiO_2 sandwich dielectric layer, such as Ta_2O_5, Y_2O_3, ZrO_2, and Ta_2O_5-Al_2O_3 proposed for 16-Mbit DRAMs,[10,11] suffer from low breakdown strengths, so that in spite of marginally respectable dielectric constants of 12–25, the effective gain in storage charge density translates to only a factor of two to three. While this might still be a viable proposition for the 64-Mbit DRAM,[12] for the 256-Mbit, 1054-Mbit, and future generations of memory cells, ferroelectric thin films have been predicted to serve as a means of scaling the DRAMs, without departing from planar processing techniques.[13] Plotted in Fig. 4 is the charge storage capacity of rapid thermally annealed PMN-PT films at 850 °C for 30 s over an applied voltage range of 2–15 V. At 5 V, the typical operating voltage for semiconductor memory, the charge capacity per unit area is 210 fC/μm^2, and surpasses the storage charge density requirement of 70–90 fC/μm^2 for a 256-Mbit MOS DRAM.[11] The films possess sufficient storage charge density even if the externally supplied voltage is reduced to 3.3 or 1.5 V, which is foreseen for memory cells with bit densities beyond 64 Mbit.[14] The charge storage capacities in Fig. 4 were determined from the nonswitching linear response derived from pulsed voltage measurements. Pulsed voltage measurements were carried out using a Sawyer–Tower circuit with a load capacitance approximately 15 times the capacitance of the ferroelectric capacitor. The pulse se-

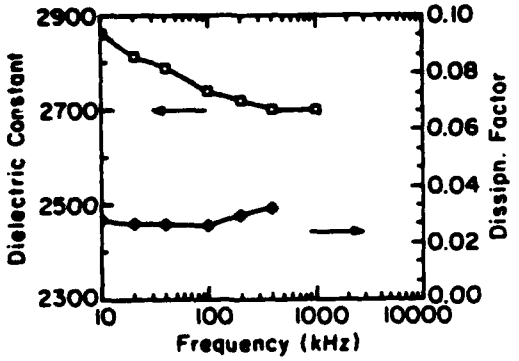

FIG. 3. Frequency dependence of the room temperature weak field dielectric constant and dissipation factor of a 0.44 μm film, annealed at 850 °C for 30 s.

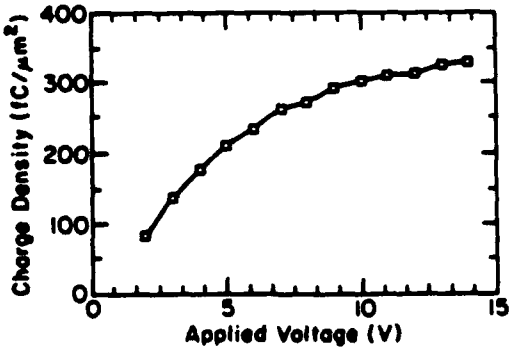

FIG. 4. The storage charge density plotted as a function of applied voltage.

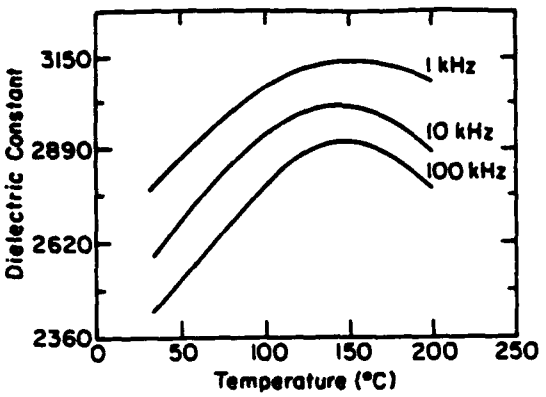

FIG. 5. The temperature dependence of the small signal dielectric permittivity of the film is plotted here. A broad maximum and a stunted permittivity at the Curie point distinguish it from a bulk ceramic; the Curie point is at about 148 °C.

quence consisted of 1 μs pulses with positive and negative bias separated by 1 s. The thin-film capacitors tested were formed by defining 100 μm $\times$ 100 μm square Pt electrodes on the annealed films. Since the relative dielectric constant of a ferroelectric is a nonlinear function of strong electric fields, the storage charge density at each field is, in effect, the difference between the displacement charge at the maximum applied electric field and zero field. This is in contrast to a nonpolar dielectric in which the storage charge density bears a linear relationship with the applied field,[15] as demonstrated recently in amorphous barium titanate films.[16] The temperature dependence of the dielectric constant is plotted in Fig. 5; the curves at different frequencies show broad maxima, with a Curie point of about 148 °C. This value is somewhat lower than that of the bulk ceramic of equivalent composition (177 °C).[1] The ferroelectric-paraelectric phase transition temperature is thus well above the commercial temperature range from 0 to 70 °C.

The large signal, hysteresis loop characteristics, including remanent polarization and coercive voltage, obtained from 60 Hz hysteresis traces (Fig. 6), were 11 μC/cm^2 and 0.5 V, respectively, for a 0.44 μm film rapid thermally annealed at 850 °C for 30 s. The large switchable polarization, and the low stable coercive voltage which is below the standard semiconductor memory supply voltage, permit reading and writing of binary information, rendering the films attractive for integrated nonvolatile memory devices.

In conclusion, ferroelectric thin films of PMN-PT of the morphotropic phase boundary composition have been shown to be potentially useful for both ferroelectric

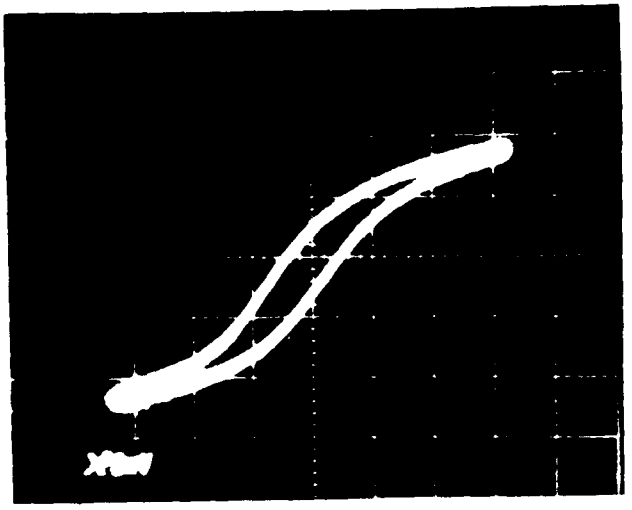

FIG. 6. Polarization-applied voltage hysteresis trace of a 0.44 μm film, rapid thermally annealed (850 °C for 30 s), at a drive frequency of 60 Hz. X-axis: 1 division = 1 V; Y-axis: 1 division = 24.6 μC/cm^2.

NVRAMs, and high density solid-state DRAMs. Determination of other important parameters that affect the performance of the films in the proposed devices is currently in progress.

[1] S. W. Choi, T. R. Shrout, S. J. Jang, and A. S. Bhalla, Ferroelectrics **100**, 29 (1989).
[2] S. L. Swartz and T. R. Shrout, Mater. Res. Bull. **17**, 1245 (1982).
[3] P. Ravindranathan, S. Komarneni, A. S. Bhalla, and R. Roy, Ferroelectric Lett. **12**, 29 (1990).
[4] L. F. Francis, Y. -J. Oh, and D. A. Payne, J. Mater. Sci. **25**, 5007 (1990).
[5] K. Okuwada, M. Imai, and K. Kakuno, Jpn. J. Appl. Phys. **28**, L1271 (1989).
[6] K. R. Udayakumar, J. Chen, V. Kumar, S. B. Krupanidhi, and L. E. Cross, in *Proceedings of the 7th IEEE International Symposium on Application of Ferroelectrics*, June 6-8, 1990, Urbana-Champaign, IL (IEEE, New York, 1991), pp. 744–746.
[7] K. R. Udayakumar, S. F. Bart, A. M. Flynn, J. Chen, L. S. Tavrow, L. E. Cross, R. A. Brooks, and D. J. Ehrlich, in *Proceedings of the 4th IEEE Workshop on Micro Electro Mechanical Systems*, Jan. 30-Feb. 2, 1991, Nara, Japan, edited by H. Fujita and M. Esashi (IEEE, New York, 1991), pp. 109–113.
[8] K. D. Budd, S. K. Dey, and D. A. Payne, Brit. Cer. Proc. **36**, 207 (1985).
[9] M. T. Goosey, A. Patel, I. M. Watson, R. W. Whatmore, and F. W. Ainger, Brit. Cer. Proc. **41**, 49 (1989).
[10] C. Hashimoto, H. Oikawa, and N. Honma, IEEE Electron Devices **36**, 14 (1989).
[11] A. F. Tasch and L. H. Parker, Proc. IEEE **77**, 374 (1989).
[12] G. Watson, IEEE Spectrum **28**, 30 (1991).
[13] B. Santo, IEEE Spectrum **26**, 47 (1989).
[14] T. Kaga, Semicond. Int. **6**, 98 (1991).
[15] L. H. Parker and A. F. Tasch, IEEE CD Mag. **6**, 17 (1990).
[16] P. Li, T. M. Lu, and H. Bakhru, Appl. Phys. Lett. **58**, 2639 (1991).

APPENDIX 38

FERROELECTRIC SWITCHING IN LEAD ZIRCONATE-LEAD ZINC NIOBATE THIN FILMS

K. R. UDAYAKUMAR, P. J. SCHUELE *, J. CHEN, K. G. BROOKS, AND L. E. CROSS

Materials Research Laboratory, The Pennsylvania State University, University Park, PA 16802
* Ramtron International Corporation, Colorado Springs, CO 80921.

ABSTRACT

Thin films of $PbZrO_3$-$Pb(Zn_{0.33}Nb_{0.67})O_3$, with PZN contents of 8-12%, were fabricated through the sol-gel spin-on technique. The structural, low frequency capacitive, and polarization reversal characteristics were investigated as a function of composition in this solid solution system. The switching of ferroelectric polarization was tested by a sequence of square wave pulses consisting of two positive pulses followed by two negative pulses. Compositions with higher PZN contents are promising for switching applications; the films were typically characterized by a switched charge of 4-14 $\mu C/cm^2$, coercive field of around 30 kV/cm, and relative permittivity of 400-800.

INTRODUCTION

Consistent with its superior dielectric and ferroelectric properties, much attention has been devoted to the development of lead zirconate titanate (PZT) thin films for radiation-hard non-volatile random access memories. In examining compositions in the solid solution system of antiferroelectric lead zirconate $PbZrO_3$ (PZ) with relaxor ferroelectric $Pb(Zn_{0.33}Nb_{0.67})O_3$ (PZN) for ferroelectric switching behavior, as in the present undertaking, the underlying motive has been to explore alternate, novel material systems for fabrication in thin film form. Takaneka et al. [1] reported good square hysteresis loop characteristics for compositions in the range 10-14% PZN, with P_r of 25-31 $\mu C/cm^2$ and E_c of 8-12 kV/cm. In this study, thin films of PZ-PZN, with PZN varying from 8-12% were prepared by the sol-gel spin-on technique; their structural and electrical characteristics were investigated.

THIN FILM PREPARATION

The sol preparation scheme for fabricating the PZ-PZN films was similar to the method used by Budd et al. [1] for fabricating PZT films. The precursors used for the synthesis of the complex alkoxides were lead acetate trihydrate, zinc acetate dihydrate, and zirconium n-propoxide, with 2-methoxyethanol as the solvent. Predetermined amounts of lead acetate trihydrate and zinc acetate dihydrate, dictated by stoichiometry and final concentration of the sol, were dissolved in the solvent in a 1:20 molar ratio at 70°C, and refluxed for 1-2 hours. The solution was double-distilled at 125°C to expel the water of hydration through a reflux condenser. The solution was then cooled to room temperature, and measured amounts of the alkoxides of Zr and Ti added. The resulting solution was refluxed under heat to allow the formation of complex alkoxides; the byproducts of the reaction were volatilized at 125°C. The concentration of the sol was then adjusted to 0.5 M. To the resulting golden yellow solution, 4% by volume of formamide was added; formamide is known to be a drying control chemical to avoid cracks in the film. Using this sol, the films were fabricated through a multi-step spin-on procedure, with intermediate pyrolysis at 400°C after each deposition for removal of the organics. Films were deposited on [100] silicon wafers with platinum electrodes sputtered on a thermally grown SiO_2 buffer layer. The films were annealed in a AG Associates Rapid Thermal Processor (Heat Pulse 210T) that can generate very high ramp rates.

FILM CHARACTERIZATION

Crystallization of the films into the proper phase was examined by X-ray diffraction. The XRD patterns of all the PZ-PZN films annealed at 850°C for 10 seconds showed single phase perovskite peaks, figure 1 being a typical XRD pattern. The microstructure of the films were examined through the scanning electron microscope; the grains were dense, with a grain size of approximately 0.5 μm (Fig. 2).

The dielectric properties of the films was measured with the aid of an impedance analyser. The small signal dielectric constant of a 0.35 μm-thick 8% PZN film was found to be 450, with a dissipation factor of 0.02. The relative permittivity increased with increase in PZN content, showing a value of 770 for 12% PZN thin film samples. The higher values of the room temperatute dielectric constant of the films compared to the bulk can possibly be attributed to the sol-gel method of preparation of the film employed in this study which is generally credited with strict compositional control and chemical homogeneity; the bulk ceramic samples in [1] were prepared by the mixed-oxide method. Fig. 3 is a representative plot of the

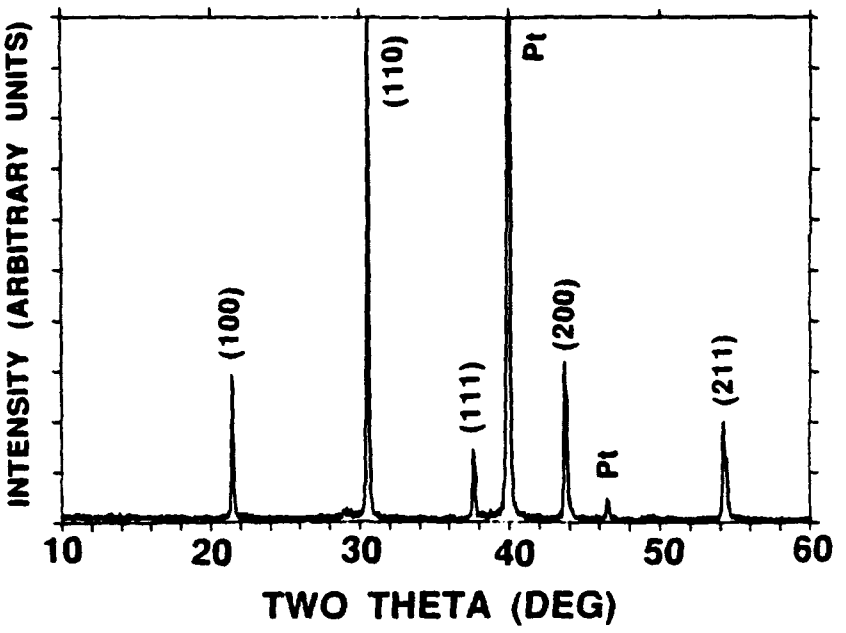

Fig. 1 XRD pattern of a 12% PZN film annealed at 850°C for 10 seconds.

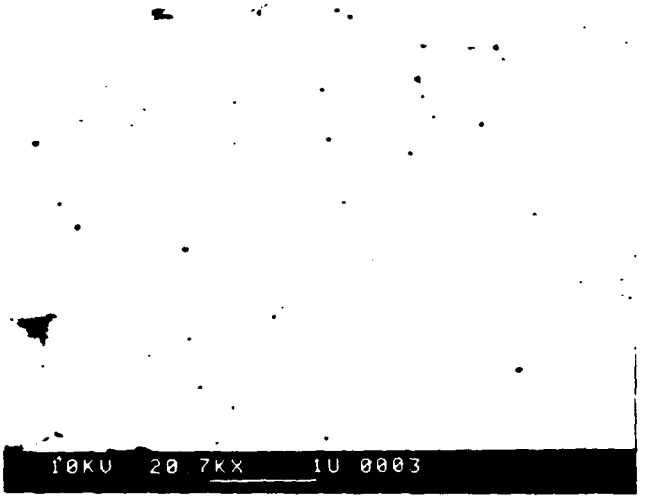

Fig. 2 Planar SEM micrograph of an annealed 12% PZN film.

dielectric constant as a function of temperature for the PZ-PZN films. For the 12% PZN films, the Curie point is at 203°C; the reported value for the bulk ceramic is 221°C [1]. Table 1 lists the dielectric properties of the other compositions.

Ferroelectric switching was measured in pulse mode. The thin film capacitors were formed by defining 100μm x 100μm square Pt electrodes on the annealed films. The pulse sequence consisted of applying two square wave pulses of 1 μsec duration of one polarity separated by 1 second, followed by two square wave pulses of opposite polarity, again separated by 1 second. The voltage was measured on the load capacitor for switched and nonswitched pulses of both polarities, and the amount of charge obtained for each pulse, $Q = C_{Load} * V$, calculated. The switching and nonswitching responses of the 12% PZN films is shown in Fig. 4. At 5 V, which is the typical circuit operating voltage for semiconductor memory applications, the amount of switched charge ($Q_{SW} = Q_N - Q_D$ or $Q_P - Q_U$) for the 12% PZN films was 12 μC/cm^2; Q_N and Q_P here indicate the switched negative and positive responses respectively, while Q_D and Q_U the unswitched negative and positive responses. The results of ferroelectric switching for the 8-12% PZN films are tabulated in Table 1. The switched charge is in the range of 4-14 μC/cm^2. This level of polarization is sufficient for the sense amplifier to accurately distinguish between a stored-one and a stored-zero in a non-volatile memory device [3,4]. From the table, notable results include the low coercive voltages (V_C) of 1 V, and low saturation voltages (V_S) of less than 5 V for these compositions.

Table I. Dielectric and ferroelectric switching characteristics of PZ-PZN thin films at varying PZN contents.

Parameter	12 % PZN	10 % PZN	8 % PZN
ε_r	770	610	450
tan δ	0.02	0.02	0.02
T_C	203°C	187°C	206°C
ε_{max}	3360	2440	1870
Q_{SW} at 5 V	11.8 μC/cm^2	4.3 μC/cm^2	5.2 μC/cm^2
V_C	1.4 V	1 V	1 V
E_C	31 kV/cm	32 kV/cm	30 kV/cm
V_S	3.6 V	3.45 V	4.5 V
E_S	78 kV/cm	111 kV/cm	129 kV/cm

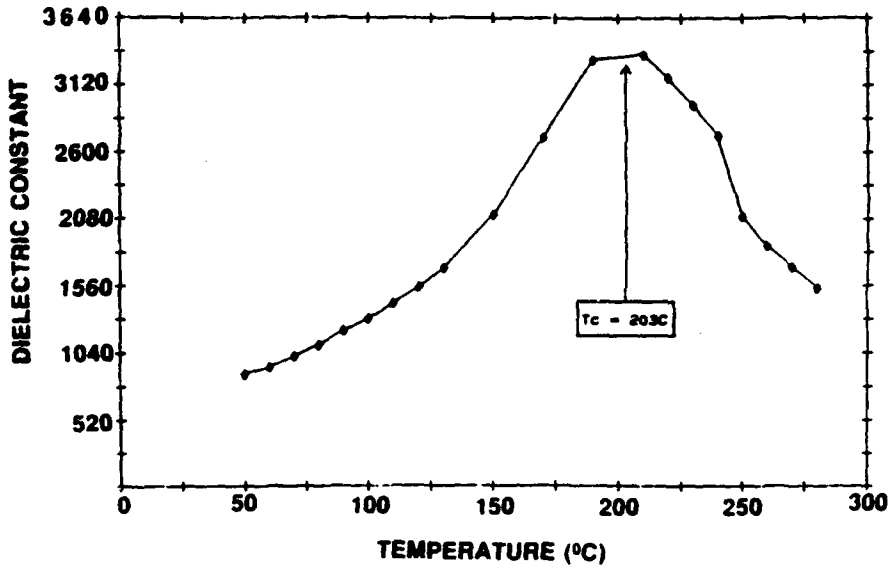

Fig. 3 High temperature dielectric behavior of 12% PZN films. The Curie point is marked in the figure.

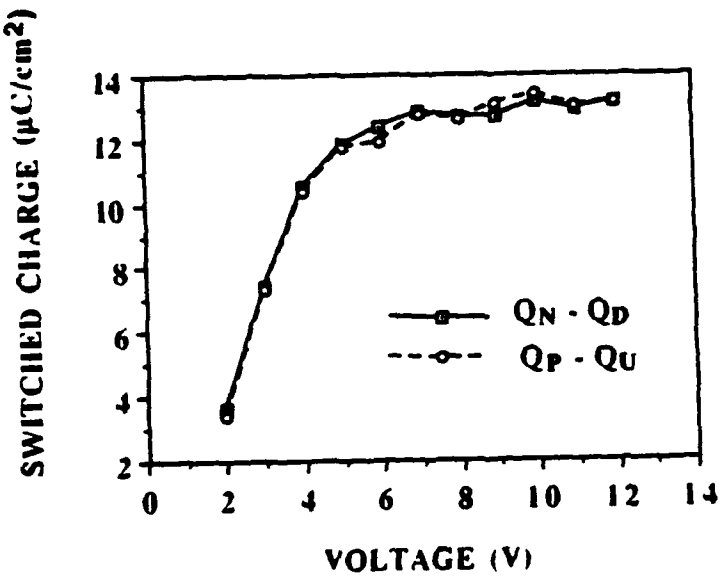

Fig. 4 Switched charge, QSW, plotted as a function of voltage for a 12% PZN film. In this film, the positive and negative responses are very close (N=P, D=U), leading to the equivalence in positive and negative switched charges.

SUMMARY AND CONCLUSIONS

This first study of the PZ-PZN system, with PZN contents varying from 8 to 12%, has shown that the films retain sufficient polarization and can be switched at very low voltages, demonstrating its potential feasibility for incorporation as storage elements in semiconductor memory devices. In the next phase of study, a broader range of compositions will be examined. Characterizing the films with higher PZN contents might reveal the trend in switching behavior. Investigating films with lower levels of PZN, extending to pure PZ, might aid in the exact location of the composition-dependent antiferroelectric-ferroelectric phase boundary; furthermore, monitoring the electric field induced antiferroelectric to ferroelectric phase switching at lower levels of PZN would be of great interest both from a scientific and technological point of view.

References

[1] T. Takaneka, A.S. Bhalla, and L.E. Cross, J. Amer. Cer. Soc., 72 (6), 1016 (1989)
[2] K.D. Budd, S.K. Dey, and D.A. Payne, Br. Cer. Proc., 36, 107 (1985)
[3] J.F. Scott and C.A. Araujo, Science, 246, 1400 (1989)
[4] W.A. Geidemann, Proceedings of the 7th IEEE International Symposium on Application of Ferroelectrics, (in press)

APPENDIX 39

LEAD ZIRCONATE TITANATE STANNATE THIN FILMS FOR LARGE STRAIN MICROACTUATOR APPLICATIONS

KEITH G. BROOKS, JIAYU CHEN, K.R. UDAYAKUMAR AND L. ERIC CROSS
Materials Research Laboratory, Pennsylvania State University, University Park, PA 16802

ABSTRACT

Thin films of antiferroelectric tetragonal $(Pb_{.97}La_{.02})(Zr_{1-x-y}Ti_xSn_y)O_3$ have been synthesized from acetate and alkoxide precursors via a sol-gel process. A multiple layer spin coating procedure was used to prepare 0.4 μm films on platinized silicon wafers. Crystallization of the films as confirmed by x-ray diffraction was achieved by rapid thermal annealing at 700°C for 20 seconds. Antiferroelectric to ferroelectric phase switching threshold fields were determined from P-E hysteresis curves. Longitudinal strain is reported as a function of applied electric field, with a maximum strain of $1.6x10^{-3}$ measured at an applied dc bias field of 120 kV/cm on a film of composition $Pb_{.97}La_{.02}(Zr_{.60}Ti_{.10}Sn_{.30})O_3$. These films show promise for micromechanical actuator applications due to the high strain associated with field forced antiferroelectric to ferroelectric phase switching.

INTRODUCTION

Research in the area of microelectromechanical systems (MEMS) has grown significantly in the past several years with applications emerging in robotics, optics, fluids, measurement and instrumentation and other areas. Electrostatic, piezoelectric, ultrasonic, shape memory and magnetic phenomenon have been exploited to produce microactuators. *Silicon micromachining, micro electro-discharge machining* and other specialized techniques have been used to produce miniature pumps, valves, microsensors and micromotors. This paper reports on the fabrication of thin films that are capable of producing actuation via an electric field forced phase transition and associated dimensional changes. One possible application of these high strain films is ultrasonic micromotors.

Microfabricated side-drive electrostatic micromotors were initially demonstrated by Fan et al. [1]. This first generation of micromotors has limited utility because of high volage requirements and inherent high rpm low torque design. Flynn et al. reported on a design for an ultrasonic micromotor that utilizes PZT thin films to achieve high torque low speed rotation [2]. The motor stator was fabricated from thin film PZT which was strained by bending with the application of a low voltage ac signal. Geardown was achieved by piezoelectrically induced ultrasonic traveling waves in the stator, coupled to the rotor by friction.

Ultrasonic micromechanical devices depend on electric field induced strain to produce actuation. For sol-gel derived PZT films, strains of $1.0x10^{-3}$ have been measured [3]. Piezoelectric ZnO has been extensively studied because of the availability of sputter deposited films. Moroney reported on the use of ZnO films to produce motion of tiny polysilicon blocks by acoustic wave agitation [4]. ZnO, however is limited because of its low dielectric constant and low achievable strain. The energy density in thin films is given by:

$$E = 1/2 \varepsilon E_{br}^2 \quad (1)$$

where ε is the relative permittivity of the dielectric and E_{br} is the electrical breakdown strength. PZT films with ε of the order of $1300\varepsilon_0$ offer a great advantage over ZnO films

with ε of $10\varepsilon_o$. Materials which undergo electric field forced phase transitions offer one possibility for achieving strains even larger than those obtained in PZT.

Electric field forced antiferroelectric (AFE) to ferroelectric (FE) phase transitions require a small free energy difference between the AFE and FE phases. Field forced transitions of this type were first demonstrated in $PbZrO_3$ over a narrow temperature range just below the 230°C Curie point [5]. A significant broadening of this temperature range was achieved by the substitution of Sn^{4+} and Ti^{4+} for Zr^{4+} in $PbZrO_3$ [6]. Substitution of La^{3+} for Pb^{2+} in $Pb(Zr_{1-x-y}Ti_xSn_y)O_3$ was shown to further reduce the free energy difference between the AFE and FE phases [7]. A schematic of the free energy relationships in this system is shown in Fig.1 [8].

Ceramics in the $Pb_{.97}La_{.02}(Zr_{1-x-y}Ti_xSn_y)O_3$ system have been extensively studied for applications including capacitive energy storage [8], shape memory [9], and high strain displacement transducers [10]. Historically, several factors have limited the usefulness of such materials. The AFE to FE transition fields are of the same range as the electrical breakdown strength of the ceramics, making such devices subject to failure. For many applications, low voltage operation is desired, and for ceramics there is a practical minimum limitation on sample thickness. Ceramic samples have also been shown to fatigue when driven through the phase transition repeatedly, with such effects being reduced in carefully polished specimens [8]. Thin films offer a unique opportunity to overcome many of these deficiencies. Breakdown strengths of greater than 1 MV/cm have been reported for sol-gel derived PZT thin films [3]. Low voltage operation is inherent to thin films, with thicknesses being less than 1 μm.

For ultrasonic micromotor applications, these materials would seem to offer many advantages. For such applications, high strain is a principal requirement. Strain levels parallel to the applied field of up to 0.85% have been reported for ceramics in the $Pb_{.97}La_{.02}(Zr_{1-x-y}Ti_xSn_y)O_3$ system [8]. Because of the nature of the strain as a function of electric field in these materials, several modes of operation are possible. Depending on composition and temperature, AFE to FE phase switching can occur as a step function or change gradually with field. These two types of transitions are characterized by 'square' and 'slanted' hysteresis loops, respectively [7]. This allows for both digital and analog mechanical motions.

For this study, three different compositions in the $Pb_{.97}La_{.02}(Zr_{1-x-y}Ti_xSn_y)O_3$ ternary system were investigated. The compositions included $Pb_{.97}La_{.02}(Zr_{.60}Ti_{.10}Sn_{.30})O_3$, $Pb_{.97}La_{.02}(Zr_{.65}Ti_{.07}Sn_{.28})O_3$ and $Pb_{.97}La_{.02}(Zr_{.65}Ti_{.0375}Sn_{.3125})O_3$ and are denoted as composition #12, #15 and #16, respectively. Fig. 2 shows the relevant portion of the ternary phase diagram with the compositions studied indicated.

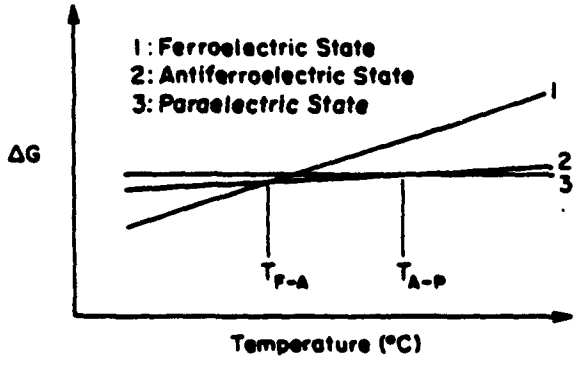

Fig.1 Free energy with paraelectric state as reference showing relative free energy difference between antiferroelectric and ferroelectric states as a function of temperature.

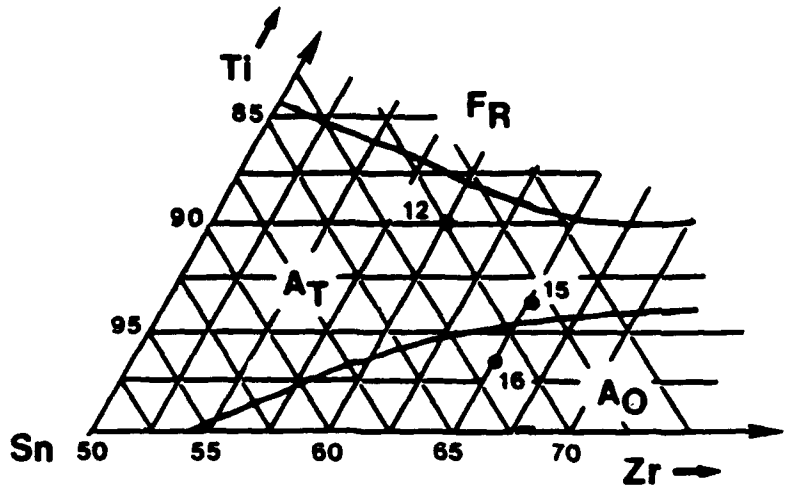

Fig.2 $Pb_{.97}La_{.02}(Zr_{1-x-y}Ti_xSn_y)O_3$ ternary phase diagram showing compositions investigated and proximity to the AFE-FE Phase boundary.

THIN FILM FABRICATION

The use of sol-gel processing for the preparation of PZT thin films was first reported by Budd et.al. [11]. In this work a similar procedure was used with modifications to include the addition of La^{3+} and Sn^{4+} cations. A predetermined quantity of $Pb(C_2H_3O_2)_2 \cdot 3H_2O$ was dissolved in anhydrous 2-methoxyethanol with heating. The water of hydration was removed by distillation following a 3 hour reflux of the solution at 80°C. Additional 2-methoxyethanol was added and the solution distilled a second time. During all phases of sol preparation, solutions were blanketed with flowing dry argon gas. Following distillation, the solution was allowed to cool to room temperature and stoichiometric quantities of anhydrous Sn^{IV} acetate and La isopropoxide were added and allowed to dissolve. To this solution, Ti isopropoxide and Zr n-propoxide were added volumetrically. The resulting solution was clear and yellow gold in color. This solution was refluxed at 80°C for several hours and then distilled at 125°C. The solution concentration was then adjusted to 0.2-0.4 M.

Thin films were prepared by a multiple layer spin coating procedure. The precursor sol solution was filtered through a 0.2 μm syringe filter prior to use. After each application the film was rapidly heated to 400°C and held for 5 minutes to facilitate removal of organics. When the desired film thickness was achieved, a rapid thermal annealing (RTA) furnace was used to crystallize the film into the perovskite structure.

Grazing angle x-ray diffraction was used to investigate the crystallinity of the annealed films. This technique maintains the source to sample angle constant, thus reducing penetration of the x-rays and increasing the diffracted intensity from the film surface. Samples annealed at 700°C for 20 seconds exhibited well crystallized perovskite diffraction patterns, as shown in Fig.3 for a film of composition #12.

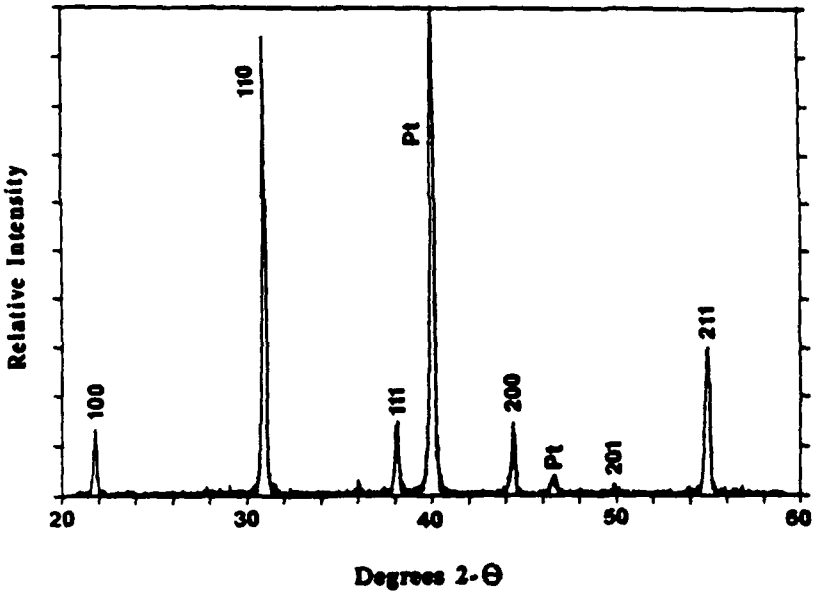

Fig. 3 Grazing angle x-ray diffraction pattern for film of composition #12.

PROPERTY MEASUREMENTS

Dielectric constants of the films were measured at 100 kHz with an ac field of ~0.25 kV/cm (10 mV) superimposed on a slowly varying dc bias. The dc bias was stepped through ~5 kV/cm (0.2 V) intervals and held for 1 second prior to capacitance measurement. The resulting double butterfly loops associated with soft antiferroelectrics were thus obtained, as shown in Fig. 4. As the dc bias field is increased, the incremental dielectric constant increases until the threshold field is reached. At this point, the permittivity decreases until a minimum at the ferroelectric saturation is observed. Upon reduction of the bias field, the permittivity again increases until reverse switching is initiated and then decreases to a zero field value which is greater than the permittivity of the virgin sample. This increase is due to poling of the sample, and is illustrated in Fig.4(b).

Dynamic polarization-electric field hysteresis curves for the various compositions are shown in Fig. 5. AFE-FE and FE-AFE switching fields were determined by taking the intersections of two lines representing the steepest and flattest sections of the hysteresis loops. Switching field data for the three compositions is provided in Table I.

Table I. Switching field and maximum polarization data for films with different applied fields.

Composition	$E_{applied}$(kV/cm)	E_{AFE-FE}	E_{FE-AFE}	P_{max}($\mu C/cm^2$)
#12	200	44	18	26.2
	300	40	20	28.8
#15	200	89	62	21.2
	300	87	59	24.7
	400	87	54	26.8
#16	800	233	134	31.5

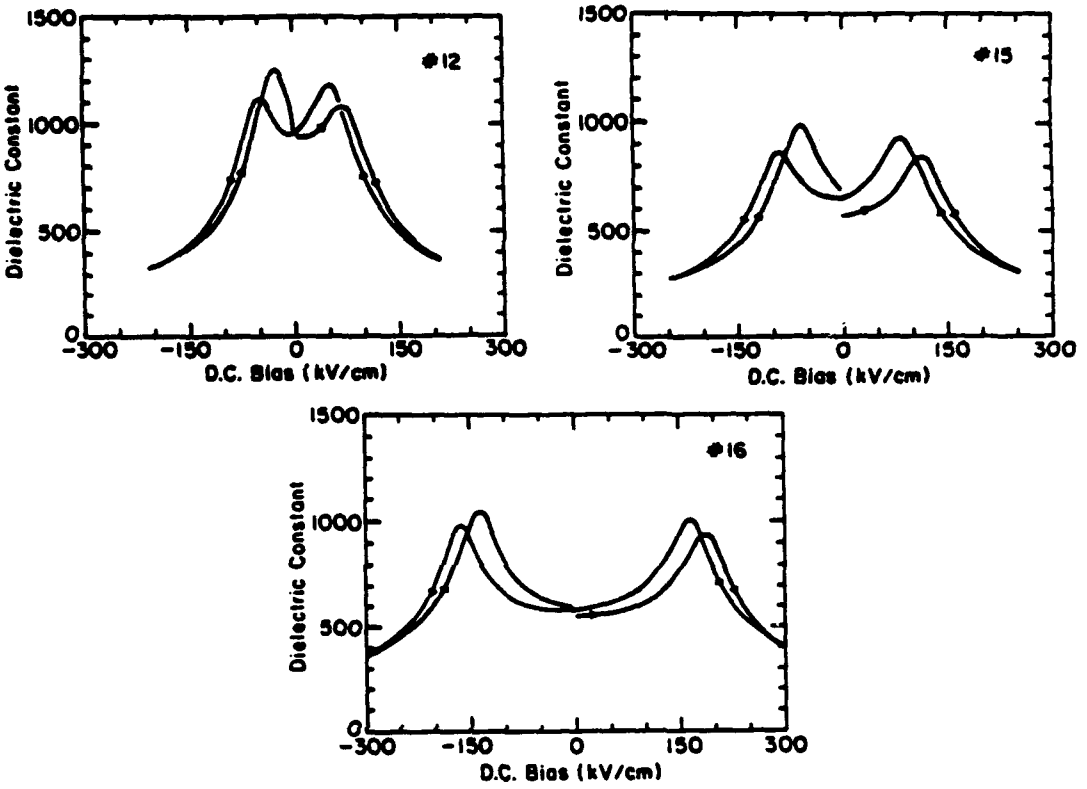

Fig.4 Permittivity as a function of slowly varying bias field for a) composition #12, b) #15 and c) #16. Curves for #12 and #16 are second iteration curves whereas #15 is a virgin curve.

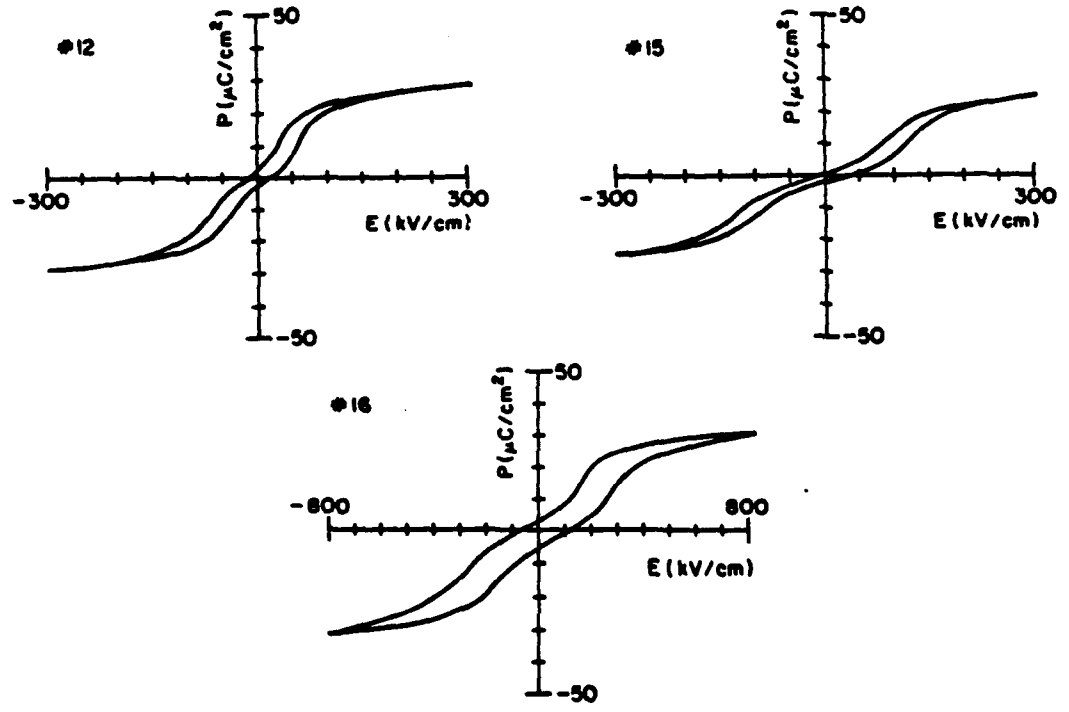

Fig.5 Polarization electric field hysteresis loops for a) compositions #12, b) #15 and c)#16.

A double beam laser interferometer with a resolution of 10^{-2} Å was used to measure longitudinal strain and has been described elsewhere [12]. Strain in a 3900 Å film of composition #12 was measured as a function of applied ac field at 500 Hz, under various dc bias conditions as shown in Fig.6. The nonlinear strain was approximated linearly at discrete applied ac fields. For the case of zero bias, the measured strain values were low because the strain oscillation frequency is two times the applied ac frequency under these conditions. The reference frequency used throughout the measurements was equal to the applied field frequency.

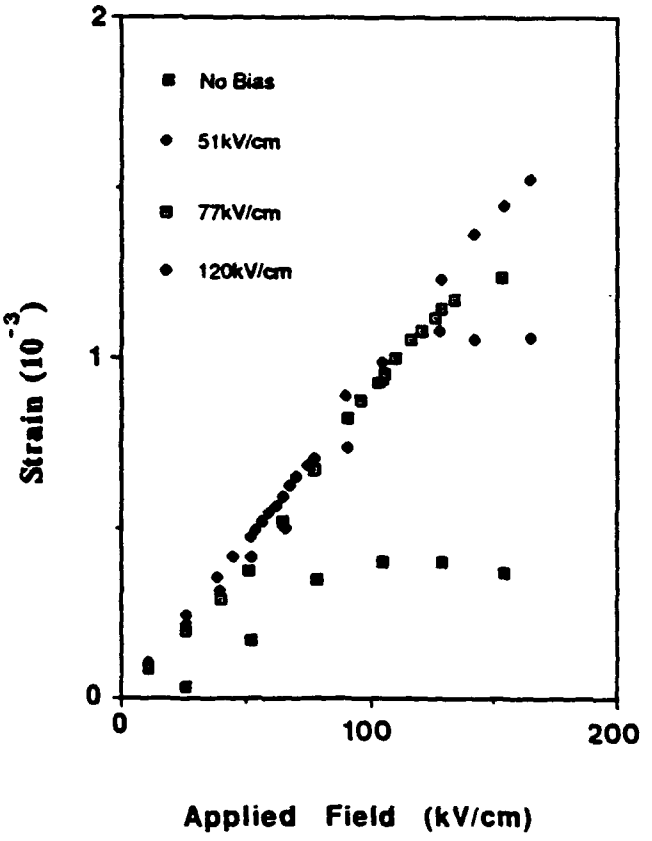

Fig.6 Strain data for composition #12 showing the effect of bias field and applied ac field.

RESULTS AND DISCUSSION

The permittivity vs. bias field data as shown in Fig. 4 clearly indicates the effect of varying the composition. Moving away from the AFE/FE phase boundary (decreasing the quantity of Ti^{4+}), caused the field at which the maximum permittivity was obtained to increase significantly. Also, the presence of hysteresis below the phase switching threshold fields is indicative of 'slanted' loop characteristic, following the observations of Berlincourt [7] on bulk $Pb_{.94}La_{.04}(Zr_{.42}Ti_{.18}Sn_{.40})O_3$ which showed similar characteristics. The transition fields were in the range 10-15 kV/cm for this bulk ceramic material. *It was shown that materials with 'slanted' loop characteristics have lower transition electric fields, lower relative volume difference between AFE and FE phase, wider temperature ranges over which the transition can occur and much less hysteresis. Furthermore, the forced transition is faster with the slanted loop material. Both types of compositions (slanted and square loop) however, exhibit similar maximum polarizations.*

Berlincourt suggested that either large ionic displacements which do no result in unit cell distortion, or much larger contributions to the polarization by electron cloud distortion rather than ionic displacement, as possible explanations for this observation.

Pan et al. [10] reported hysteresis data for bulk ceramics of composition #12 which is more characteristic of a square loop material. The longitudinal strain reported for the bulk material was 4.2×10^{-3} compared to 1.6×10^{-3} for the thin film (Fig. 6) with an applied field three times larger than used for the bulk measurement. However, AFE-FE transition fields were comparable, being ~44 and 49 for thin film and bulk samples, respectively. Maximum polarization values were also comparable, ~32 and 29 $\mu C/cm^2$ for bulk and thin film, respectively.

It is possible that residual stresses from thermal expansion mismatch between the film and the platinum substrate have an effect on the strain properties of these films.

CONCLUSIONS

Thin films in the tetragonal $PbLa(Zr_{1-x-y}Ti_xSn_y)O_3$ system have been fabricated which show large strain characteristics due to AFE-FE phase transition. Such films are suitable for micromechanical systems where high relative strain and low voltage are required.

ACKNOWLEDGMENT

The authors thank Ms. Hong Wong for assistance with the strain measurements.

REFERENCES

[1] L.S Fan, Y.C. Tai and R.S. Muller, Proc. IEEE Int. Electr. Devices Meeting, San Francisco, CA 666 (1988).
[2] A.M. Flynn, L.S. Tavrow, S.F. Bart, R.A. Brooks, D.J. Ehrlich, K.R. Udayakumar and L. E. Cross, IEEE Ultrasonics Symp., Honolulu, Hawaii, 1163 (1990).
[3] K.R. Udayakumar, J. Chen, S.B. Krupanidhi, and L.E. Cross, Proc. 7th Int. Symp. Appl. Ferroelectrics, June 8-9 1990, Champaign-Urbana, IL, 741 (1991).
[4] R.M. Moroney, R.M. White and R.T. Howe, Proc. IEEE MEMS, Napa Valley, CA 182 (1990).
[5] G. Shirane, E. Sawaguchi, and Y. Takagi, Phys. Rev. 84 476 (1951).
[6] E. Sawaguchi, J. Phys. Soc. Japan 8 615 (1951).
[7] D. Berlincourt, IEEE Trans. Sonics Ultrasonics SU-13 116 (1966).
[8] W. Y. Pan, C. Q. Dam, Q. M. Zhang and L.E. Cross, J. Appl. Phys. 66 6014 (1989).
[9] K. Uchino and S. Nomura, Ferroelectrics 50 517 (1987).
[10] W. Pan, Q. Zhang, A Bhalla and L.E. Cross, J. Am. Ceram. Soc. 72 571 (1989).
[11] K.D. Budd, S.K. Dey and D.A. Payne, Brit. Ceram. Proc. 36 107 (1985).
[12] Q.M. Zhang, W.Y. Pan and L.E. Cross, Ferroelectrics 89 (1989).

APPENDIX 40

FERROELECTRIC THIN FILM ULTRASONIC MICROMOTORS

K. R. Udayakumar [1], S. F. Bart [2], A. M. Flynn [2], J. Chen [1],
L. S. Tavrow [2], L. E. Cross [1], R. A. Brooks [2], D. J. Ehrlich [3]

[1] Materials Research Laboratory, Pennsylvania State University, University Park, PA
[2] MIT Artificial Intelligence Laboratory, Cambridge, MA
[3] MIT Lincoln Laboratory, Lexington, MA

ABSTRACT

Ferroelectric thin films of lead zirconate titanate (PZT) of the morphotropic phase boundary composition have been fabricated for application to a new family of flexure-wave piezoelectric micromotors that are characterized by low speed and high torque. The high relative dielectric constant (1300) and breakdown strength (1 MV/cm) of the films lead to high stored energy densities. The piezoelectric coefficients d_{33} and d_{31} were measured to be 220 pC/N and -88 pC/N respectively; the electromechanical coupling factors calculated thereupon were k_{33}=0.49, k_{31}=0.22, and k_p=0.32. The development of the piezoelectric ultrasonic micromotors from the PZT thin films, and the architecture of the stator structure are described. Nonoptimized prototype micromotors show rotational velocities of 100-300 rpm, and net normalized torques in the pN-m/V^2 range.

1. INTRODUCTION

The last five years have seen an expanding quantity of work on microfabricated actuators. A great deal of the effort has been centered around the electrostatic rotary micromotor [1-3] which, however, has fundamental limitations. First, its planar structure makes it difficult to couple mechanical power, especially out of the plane of the rotor. Second, the basic variable-capacitance design is inherently a high speed, low torque, synchronous motor. In addition, frictional forces have been shown to be a significant limitation [4,5].

This paper describes work on materials and initial structures for an ultrasonic microfabricated motor. Ultrasonic micromotors may overcome some of the difficulties associated with electrostatic micromotors [6]. Macroscopic ultrasonic motors have been developed previously and have found commercial niches [7]. Motions of small polysilicon blocks have been observed in microfabricated structures using films of ZnO [8]. Also, molecular transport has been demonstrated [9]. The major advantages of ultrasonic drives for micromotors along with our initial experiments on thin film PZT actuators are described in Reference 10.

A typical ultrasonic motor develops high torque at low speed because of the inherent gear down from the piezoelectrically induced ultrasonic travelling wave velocity on the stator to the rotor velocity [7]. Frictional contact between the rotor and the stator is required for this mechanical force transduction. This friction dominated drive mechanism may reduce the complexity of coupling mechanical power out. It also provides a holding torque even in the absence of applied power. The drawback of this type of operation is that the normal force applied between the rotor and the stator must be controlled to obtain optimum performance. Also, wear due to the frictional coupling must be controlled.

It has been argued that a simple, but useful measure of an electromechanical transducer's ability to provide torque is its stored electric energy [11]. A typical 100-μm radial-gap variable-capacitance micromotor has a stored energy density of about 5×10^4 J/m^3, assuming a typical maximum voltage of 100 volts applied across a rotor-stator air gap of 1 μm. In the piezoelectric micromotor, the rotor-stator gap consists of a thin film of piezoelectric material. In the structures to be described here, films of lead zirconate titanate (PZT) are deposited typically with thicknesses of around 0.4 μm. The relative dielectric constant of these films, as evident in the next section, is about 1300. Assuming an applied potential of 5 volts across the film, the stored energy density is about 9×10^5 J/m^3. To compare the actual stored energy, these values must be multiplied by the volume in which the electric field is applied. Since the ultrasonic motor is inherently an axial-gap structure, this volume will be much larger than the volume in a radial-gap variable-capacitance micromotor. Clearly, then, the high dielectric constant of PZT and the ultrasonic motor's axial-gap design gives the ultrasonic motor the potential to provide significantly more work, even while using a significantly lower applied voltage.

Previous work on ultrasonic micromotors has used zinc oxide as the piezoelectric material [8] due to its ease of fabrication. However, lead zirconate titanate (PZT) has been chosen in this work because of its high dielectric and piezoelectric constants, as compared to ZnO. These properties yield a larger stored energy density and strain which offer the possibility of significantly larger torques at lower excitation voltages.

Attempts at fabrication of PZT thin films by vacuum deposition methods have hitherto been hampered by difficulties in controlling the film stoichiometry. A sol-gel spin-on technique, based on our earlier work [12], has been employed in this study. In the next section, we briefly describe the solution synthesis and film fabrication; the dielectric, piezoelectric and ferroelectric properties of the PZT films of the morphotropic phase boundary composition are then presented. The films exhibit physical properties that parallel those of the bulk ceramic of equivalent composition. Finally, we describe the preliminary development of the ultrasonic micromotor in Section 3.

CH2957-9/91/0000-0109$01.00

2. THIN FILM FABRICATION AND PHYSICAL PROPERTIES

2.1 Film Fabrication

In brief, the sol preparation involves the following steps. Lead acetate trihydrate is dissolved in 2-methoxyethanol at 70 °C and refluxed. The water of hydration from this Pb precursor is distilled through a reflux condenser to facilitate the addition of moisture sensitive alkoxides of Ti and Zr. The byproducts of the reaction are expelled, following prolonged refluxing, at 80 °C. The solution is then partially hydrolysed, and a controlled amount of acid or base added as catalyst. Films were fabricated by a multi-step spin-on technique, with pyrolysis at 400 °C after each step to remove the organics. Films were built up to the desired thickness, and then crystallized to obtain the perovskite by annealing at temperatures above 500 °C. Structural characterization of the films were carried out by X-ray diffraction.

2.2 Physical Properties

In this subsection, the dielectric, piezoelectric and ferroelectric properties of the PZT films at the morphotropic phase boundary composition will be discussed. Only those aspects of the ferroelectric properties that are relevant to the micromotor development will be dealt with here; detailed discussion of other aspects may be found elsewhere [12].

The factors that influence the stored energy density are the relative dielectric constant and the ability of the films to withstand high electric fields. Fig. 1 shows the room temperature weak-field relative permittivity of the films reach high values of 1300, with low dissipation losses of 0.03, beyond a film thickness of 0.3 μm. This represents an increase of 2 orders of magnitude over the dielectric constant of ZnO. From Fig. 2, the breakdown strength of the films are over 1 MV/cm, as compared to 60-80 kV/cm for the bulk ceramic.

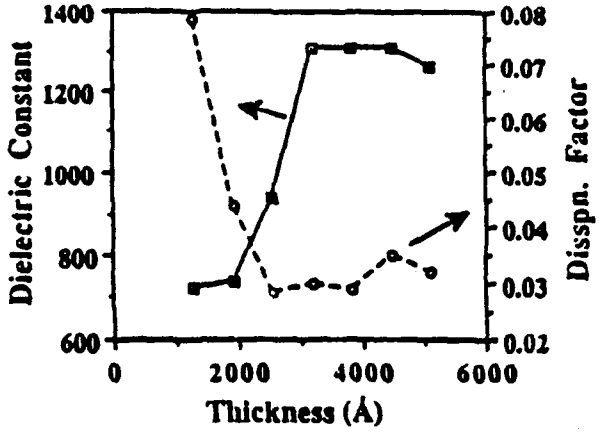

Fig. 1 The room temperature weak-field permittivity is plotted here as a function of film thickness, at 10 kHz. Note that the dielectric permittivity is independent of film thickness beyond 3 μm.

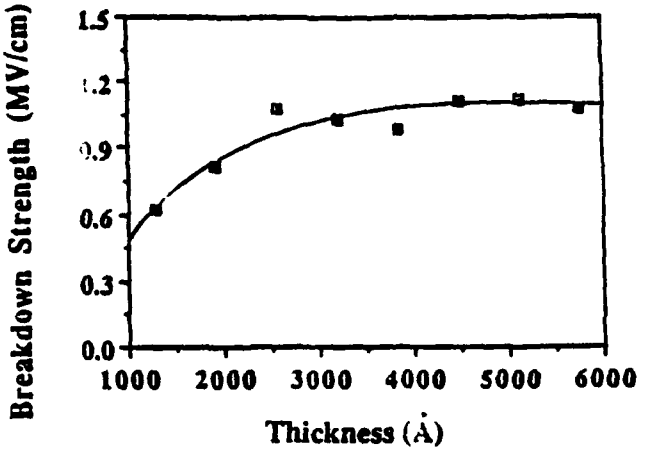

Fig. The dielectric breakdown strength of the films is over 1 MV/cm. In comparison, the bulk ceramic has a value of 60-80 kV/cm.

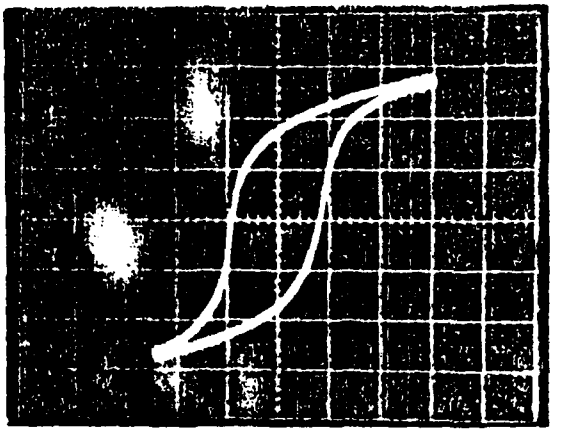

Fig. 3 The polarization-electric field hysteresis loop of a 0.45-μm-thick PZT film at 60 Hz is shown. The trace above is at an applied electric field of 120 kV/cm.

Fig. 3 represents the characteristic polarization reversal of a ferroelectric, and was traced for a 0.45-μm-thick PZT film with the aid of a modified Sawyer-Tower circuit. A large switchable electric polarization of 35 μC/cm² was calculated from the symmetric hysteresis loop. This value of remanent polarization. P_r, is pertinent here since it bears a linear dependence to the longitudinal piezoelectric coefficient, d_{33}.

The piezoelectric coefficients, d_{33} and d_{31}, were measured by a small signal strain technique using a laser interferometer which has the capability to resolve an ac electric field induced displacement of the order of 10^{-13} m [13]. Fig. 4 represents the strain response of a 0.45-μm-thick PZT film at 1 kHz driving field with a 72 kV/cm dc bias. The longitudinal piezoelectric coefficient, d_{33}, is calculated through the converse piezoelectric effect, described by $s_3=d_{33}E_3$ (reduced tensor notation), where s_3 represents the strain and E_3 the electric field. d_{33} was found to vary with dc bias (Fig. 5), with a peak value of 220 pC/N at 75 kV/cm. This compares to 223 pC/N reported for an undoped PZT ceramic of equivalent composition [14]. The trend in Fig. 5 is an apparent reflection of the dielectric response to the dc bias, shown in Fig. 6; d_{33} is related to the remanent polarization, P_r, the electrostrictive constant, Q_{11}, and the dielectric permittivity, ε_{33}, through $d_{33}=2Q_{11}P_r\varepsilon_o\varepsilon_{33}$.

To measure the transverse piezoelectric coefficient, d_{31}, the film was used as a piezoelectric flexure element, or bimorph, in which the film is considered to be bonded to the Si substrate. A piezoelectric strip, of length ten times the width, was used as a bimorph, and a voltage difference applied across its conducting surfaces. This results in an interior electric field that stresses and strains the bimorph, leading to a deformation. Fig. 7 is a plot of the displacement of the bimorph, with a 0.38-μm-thick PZT film, as a function of the ac field. Using stress analysis, the piezoelectric transverse coefficient, d_{31}, was derived by relating the quasistatic deflection of the heterogeneous wafer-film structure to the geometry and piezo/elastic parameters of its components, and the driving electric field. At an ac field of 200 kV/cm, d_{31} was calculated to be -88.7 pC/N, a magnitude close to -93.5 pC/N of the bulk ceramic [14].

The electromechanical coupling factors measure the square root of the fraction of the electrical energy converted to mechanical energy in each cycle, and are dimensionless measures of the strength of the piezoelectric effects. The commonly used coupling factors, k_{33}, k_{31}, and k_p, derived from the equations of state, are given by [14]:

$$k_{33} = d_{33} / (\varepsilon_o \varepsilon_{33}^T s_{33}^E)^{0.5}$$

$$k_{31} = d_{31} / (\varepsilon_o \varepsilon_{33}^T s_{11}^E)^{0.5}$$

$$k_p = d_{31} / (2 / \varepsilon_o \varepsilon_{33}^T (s_{11}^E + s_{12}^E))^{0.5}$$

While the dielectric and piezoelectric constants for the films are known from above, the elastic constants of the bulk ceramic are assumed to hold for the films ($s_{11}^E = 138 \times 10^{-12}$, $s_{33}^E = 17.1 \times 10^{-12}$, $s_{12}^E = -4.07 \times 10^{-12}$ m²/N). Incorporating these values, k_{33}=0.49, k_{31}=0.22, and k_p=0.32.

The d_{33} and d_{31} measured above constitute the first reported piezoelectric coefficients and electromechanical coupling coefficients for PZT thin films. An extensive comparitive study of the dielectric and ferroelectric properties of the PZT films by a number of vacuum deposition methods has been undertaken in Reference 12. From this data, the dielectric constant of the sol-gel films appear to be superior to the films fabricated by rf diode sputtering (750), planar magnetron sputtering with multi-element metal targets (200), rf magnetron sputtering yielding epitaxial films (400), ion beam deposition (125), and thermal decomposition of organo-metallic compounds (300) by a factor of 1.5 to 10. There has been no data on the breakdown strengths of PZT thin films hitherto.

3. MICROMOTOR DEVELOPMENT

Fig. 8 shows a scanning electron micrograph cross-section of the micromotor stator structure. To fabricate these, 1 μm of low-stress silicon-rich silicon nitride was deposited on silicon wafers. These wafers were back-side etched to form diaphragms over several millimeter square through wafer vias. Platinum was then deposited on these diaphragms to form a nonoxidizing ground plane. A 20-nm-thick titanium layer was used for adhesion of Pt to the nitride diaphragm. The PZT films were then fabricated as described in Section 2. The upper stator electrodes are gold, patterned by a lift-off process. This stator electrode pattern can be seen in Fig. 9 which also shows a glass rotor in position on the stator structure.

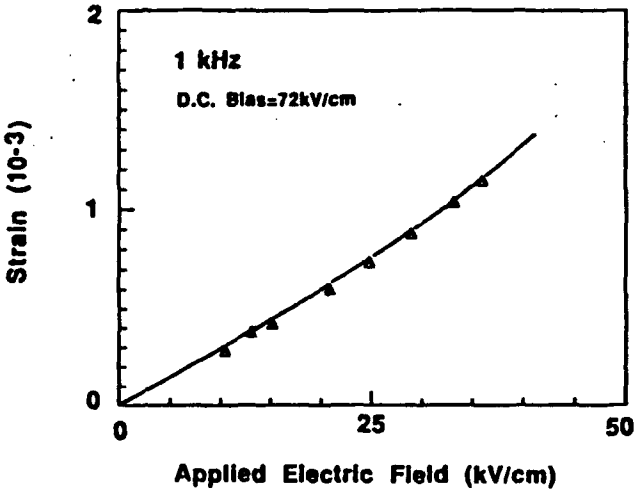

Fig. 4 The longitudinal piezoelectric coefficient, d_{33}, is obtained from the slope of the strain-applied field plot. The above plot is for a 0.45-μm-thick PZT film with a 72 kV/cm dc bias at 1 kHz.

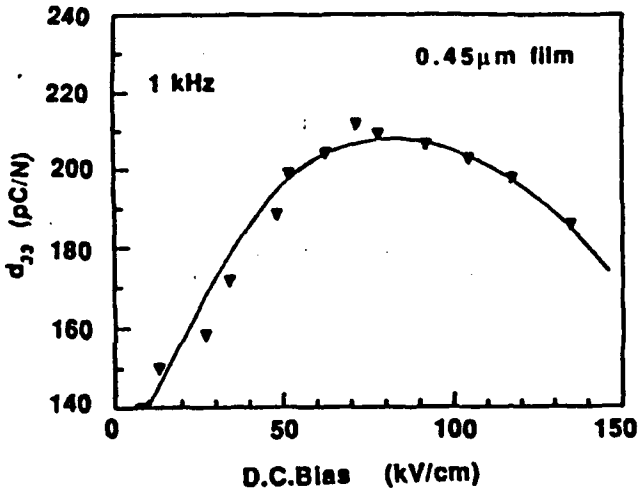

Fig. 5 d_{33} obtained from the previous figure is plotted as a function of the dc bias at the same frequency.

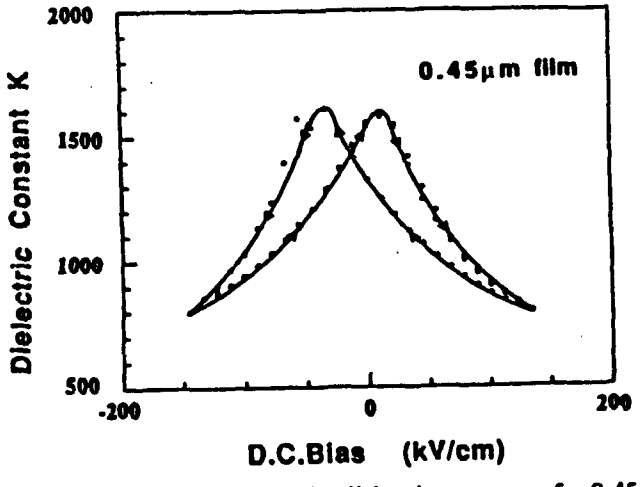

Fig. 6 This plot illustrates the dielectric response of a 0.45-μm-thick PZT film to the probing field.

Rotary motion of the glass rotor in the system shown in Fig. 9 has been demonstrated for the case of a single-phase excitation in the range of 60-100 kHz and applied voltages of 3 to 4 volts peak-to-peak. Preliminary results yield a net normalized torque, based on the net acceleration of the rotor, of 1.6×10^{-12} N-m/V^2, which is significantly larger than

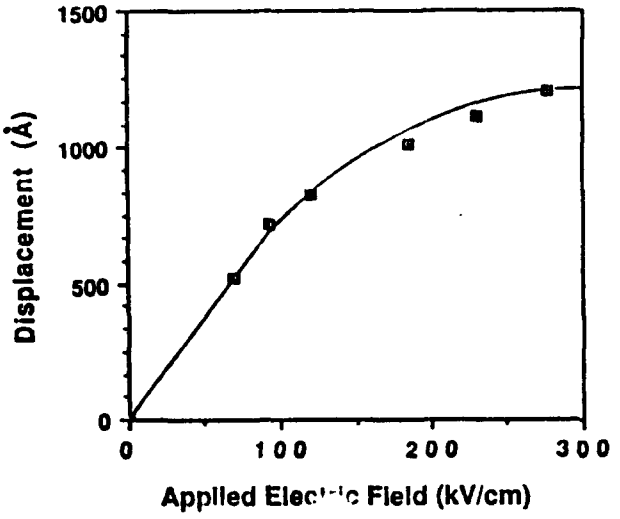

Fig. 7 The film is used as a piezoelectric flexure element to measure d_{31}. Recorded above is the displacement of the bimorph on application of an ac field, constituting the raw data for calculating d_{31}.

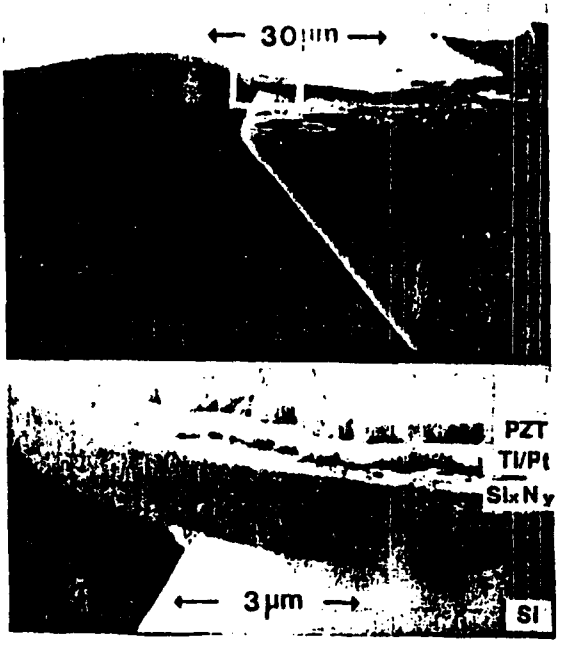

Fig. 8 The SEM photograph above is a cross-section of the PZT micromotor structure.

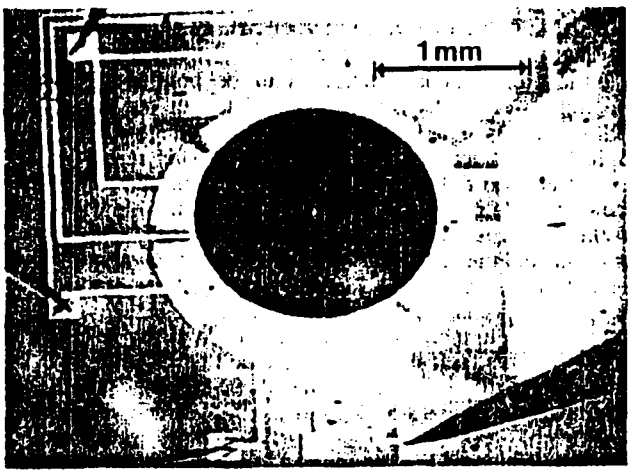

Fig. 9 A lens of 1.5 mm diameter placed atop the 8-pole rotary stator, as shown in this figure, spins at a velocity of 100-300 rpm for a 2-4 V peak-to-peak drive signal at 60-100 kHz.

1.4×10^{-15} N-m/V^2, a value typical for electrostatic micromotors [4]. This rotary motion is assumed to be the result of coupling to the standing wave vibration patterns in a nonoptimized way. It is believed that the coupling will improve significantly when a true travelling wave excitation can be applied. Also, gravity is the only normal force acting between the rotor and the stator in this system, again yielding nonoptimized mechanical coupling.

A simple estimate for the strain energy density in the film is given by $1/2E\varepsilon^2$ where E is the Young's modulus and ε is the strain. Assuming that the strain induced in the PZT film is also induced in the silicon nitride membrane, and that the strain energy density in the thin PZT film is small compared to the silicon nitride membrane, strains on the order of 10^{-3} (Fig. 4) yield a strain energy density in the silicon nitride on the order of 6×10^5 J/m^3. This value is quite similar to the electric stored energy density calculated above.

4. CONCLUSIONS

Through a sol-gel spin-on technique, single-phase, stoichiometric, adherent PZT thin films of the morphotropic phase boundary composition have been fabricated for application to the development of piezoelectric ultrasonic micromotors; the relevant dielectric, ferroelectric and piezoelectric properties thereof have been discussed. The high relative dielectric constant and breakdown strengths of the films lead to high stored energy densities, which translates to lower driving voltages of 2-4 volts for ultrasonic micromotors, compared to hundreds of volts as in an air-gap electrostatic micromotor. The measured piezoelectric coefficients, d_{33} and d_{31}, are 220pC/N and -88pC/N respectively, close to the bulk values.

This work has clearly demonstrated the potential of a piezoelectric ultrasonic micromotor by combining ferroelectric thin films with silicon micromachining. Nonoptimized micromotors have displayed rotary motion, characterized by low rotational velocities of 100-300 rpm, and net normalized torques of the order of pN-m/V^2.

ACKNOWLEDGMENTS

The authors gratefully acknowledge the financial support received in part from the Gnat Robot Corporation and in part from the University Research Initiative under Office of Naval Research contract N00014-86-K-0685. The Lincoln Laboratory portion of this work was supported by the Department of the Air Force, in part by a specific program from the Air Force Office of Scientific Research. We are indebted to Chester A. Bukowski, who performed much of the metallization and other fabrication at Lincoln Laboratory.

REFERENCES

[1] M. Mehregany, S.F. Bart, L.S. Tavrow, J.H. Lang, and S.D. Senturia, "Principles in Design and Microfabrication of Variable-Capacitance Side-Drive Motors," *J. Vac. Sci. and Tech.*, vol. A8, 3614-24 (1990).

[2] L.S. Fan, Y.C. Tai, and R.S. Muller, "IC-Processed Electrostatic Micromotors," *Sensors and Actuators*, vol. 20, 41-47 (1989).

[3] L.S. Tavrow, S.F. Bart, M.F. Schlecht, and J.H. Lang, "A LOCOS Process for an Electrostatic Microfabricated Motor," *Sensors and Actuators*, vol. A23, 893-898 (1990).

[4] S.F. Bart, M. Mehregany, L.S. Tavrow, J.H. Lang, and S.D. Senturia, "Measurements of Electric Micromotor Dynamics, "*Microstructures, Sensors and Actuators*, ASME, Dallas, TX, DSC-GOL.19, AR19-29 (1990).

[5] Y.C. Tai and R.S. Muller, "Frictional Study of IC-Processed Micromotors," *Sensors and Actuators*, vol. A21, 180-183 (1990).

[6] A.M. Flynn, R.A. Brooks, and L.S. Tavrow, "Twilight Zones and Cornerstones: A Gnat Robot Double Feature", *MIT A.I. Memo 1126*, July 1989.

[7] R. Inaba, A. Tokushima, O. Kawasaki, Y. Ise, and H. Yoneno, "Piezoelectric Ultrasonic Motor," *Proceedings of the 1987 IEEE Ultrasonics Symposium*, 747-756 (1987).

[8] R.M. Moroney, R.M. White, and R.T. Howe, "Ultrasonic Micromotors: Physics and Applications," *Proceedings of the 3rd IEEE Workshop on Micro Electro Mechanical Systems*, Napa Valley, CA, 182-187 (1990).

[9] P. Terry and M.W.P. Strandberg, "Induced Molecular Transport due to SAW," *J. Appl. Phys.*, vol. 52, no. 6, 4281-87 (1981).

[10] A.M. Flynn, L.S. Tavrow, S.F. Bart, R.A. Brooks, D.J. Ehrlich, K.R. Udayakumar, and L.E. Cross, "Piezoelectric Micromotors for Microrobots", *IEEE Ultrasonics Symposium*, Dec 4-7, 1990 at Honolulu, Hawaii.

[11] S.F. Bart, T.A. Lober, R.T. Howe, J.H. Lang, and M.F. Schlecht, "Design Considerations for Microfabricated Electric Actuators," *Sensors and Actuators*, vol. 14, no. 3, 269-292 (1988).

[12] K.R. Udayakumar, J. Chen, S.B. Krupanidhi, and L.E. Cross, "Sol-Gel Derived PZT Thin Films for Switching Applications," *Proceedings of the 7th International Symposium on Application of Ferroelectrics*, June 6-8, 1990 at Urbana-Champaign, Ill.

[13] Q.M. Zhang, W.Y. Pan, and L.E. Cross, "Laser Interferometer for the Study of Piezoelectric and Electrostrictive Strains", *J. Appl. Phys.*, 2492-96 (1988).

[14] B. Jaffe, W.R. Cook and H. Jaffe, *Piezoelectric Ceramics*, (Academic Press, 1971).

APPENDIX 41

Piezoelectric Micromotors for Microrobots

Anita M. Flynn, *Member, IEEE*, Lee S. Tavrow, *Member, IEEE*, Stephen F. Bart, *Member, IEEE*, Rodney A. Brooks, *Member, IEEE*, Daniel J. Ehrlich, *Member, IEEE*, K. R. Udayakumar, and L. Eric Cross, *Fellow, IEEE*

***Abstract*—Mobile robots are able to carry more and more intelligence (and in smaller packages) on board everyday. There is a need, however, for smaller actuators to make these machines more dextrous, compact, and cost effective. Toward this end, we have begun research into piezoelectric ultrasonic motors using ferroelectric thin films. We have fabricated the stator components of these millimeter diameter motors on silicon wafers. Ultrasonic motors consist of two pieces: a stator and a rotor. The stator includes a piezoelectric film in which we induce bending in the form of a traveling wave. Anything which sits atop the stator is propelled by the wave. A small glass lens placed upon the stator becomes our spinning rotor. Piezoelectric micromotors overcome the problems currently associated with electrostatic micromotors such as low torque, friction, and the need for high voltage excitation. More importantly, they may offer a much simpler mechanism for coupling power out. Using thin films of lead zirconate titanate on silicon nitride membranes, various types of actuator structures can be fabricated. By combining new robot control systems with piezoelectric motors and micromechanics, we propose creating micromechanical systems that are small, cheap and completely autonomous.**

I. Smaller and Smaller

TODAY's robots are large, expensive, and not too clever. Robots of the future may be small and cheap (and perhaps still not too clever). But if we could achieve even insect level intelligence while scaling down sizes and costs, there may be tremendous opportunities for creating useful robots. From autonomous sensors to robots cheap enough to throw away when they have completed their task—microrobots provide a new way of thinking about robotics.

Our goal of building gnat-sized robots has been driven by recent successes in developing intelligence architectures for mobile robots which can be compiled efficiently into parallel networks on silicon. Brooks' subsumption-style architectures [6] provide a way of combining distributed real time control with sensor-triggered behaviors to produce a variety of robots exhibiting "insect level" intelligence [7], [2], [8], [18], [10], [17]. This assemblage of artificial creatures includes soda can collecting robots, sonar-guided explorers, six-legged arthropods that learn to walk, and a "bug" that hides in the dark and moves toward noises.

One of the most interesting aspects of the subsumption architecture has to do with the way it handles *sensor fusion*, the issue of combining information from various, possibly conflicting, sensors. Typically, sensor data are fused into a global data structure, and robot actions are planned accordingly. A subsumption architecture, however, instead of making explicit judgements about sensor validity, encapsulates a strategy that might be termed *sensor fission*, whereby sensors are dealt with only implicitly in that they activate behaviors. Behaviors are just layers of control systems that all run in parallel whenever appropriate sensors fire. The problem of conflicting sensor data then is handed off to the problem of conflicting behaviors. "Fusion" consequently is performed at the output of behaviors (*behavior fusion*) rather than the output of sensors. A prioritized arbitration scheme then selects the dominant behavior for a given scenario.

The ramification of this distributed approach to handling vast quantities of sensor data is that it takes far less computational hardware. Since there is no need to handle the complexities of maintaining and updating a map of the environment, the resulting control system becomes very lean and elegant.

The original idea for gnat robots [9] came about when the realization that subsumption architectures could compile straightforwardly to gates coincided with a proposal [4] to fabricate an electrostatic motor on a chip (approximately 100 μm in diameter). Early calculations for this silicon micromotor forecast small but useful amounts of power. Already, many types of sensors (i.e., imaging sensors, infrared sensors, force sensors) microfabricated on silicon are commercially available. If a suitable power supply could be obtained (solar cells are silicon and thin film batteries are beginning to appear in research laboratories), the pieces might begin to fit.

The driving vision is to develop a technology where complete machines can be fabricated in a single process,

Manuscript received July 10, 1991; revised October 18, 1991. Subject Editor D. Cho. This work was supported in part by the Gnat Robot Corporation, in part by the University Research Initiative under Office of Naval Research Contract N00014-86-K-0685, and in part by the Department of the Air Force, by a specific program from the Air Force Office of Scientific Research.

A. M. Flynn and R. A. Brooks are with the Artificial Intelligence Laboratory, Massachusetts Institute of Technology, Cambridge, MA 02139.

L. S. Tavrow was with the Artificial Intelligence Laboratory, Massachusetts Institute of Technology, Cambridge, MA. He is now with Sun Microsystems Inc., Mountain View, CA 94043.

S. F. Bart was with the Artificial Intelligence Laboratory, Massachusetts Institute of Technology, Cambridge, MA. He is now with the Bose Corporation, Framingham, MA 01701.

D. J. Ehrlich is with the Lincoln Laboratory, Massachusetts Institute of Technology, Lexington, MA 02173.

K. R. Udayakumar and L. E. Cross are with the Materials Research Laboratory, Pennsylvania State University, University Park, PA 16802.

IEEE Log Number 9105260.

alleviating the need for connectors and wiring harnesses and the necessity for acquiring components from a variety of vendors as would be found in a traditional large-scale robot. The microrobots would be designed in software through a "robot compiler," and a foundry would convert the files to masks and then print the robots en masse. One critical technology presently missing is a batch-fabricatable micromotor which can couple useful power out to a load.

Various types of intriguing microactuators have recently appeared. One example is the variable capacitance silicon electrostatic motor (which is based on the force created due to charge attraction as two plates move past each other) [24], [12], [19]. Fig. 1 illustrates one such electrostatic micromotor. Another type of micromotor is a "wobble" motor, where one cylinder precesses inside another, again due to electrostatic forces [14], [26]. Fig. 2 illustrates a wobble motor. In general, electrostatic motors are preferred over magnetostatic motors in the microworld because electrostatic forces scale favorably as dimensions shrink and because dielectric materials are more easily patterned and processed than magnetic materials, especially in the realm of silicon processing. The three-dimensional windings required for magnetostatic motors would be very hard to fabricate in silicon, but the small gap sizes that allow electrostatic motors to take advantage of the ability to withstand increased electric fields before breakdown are easily fabricated using photolithographic techniques. Electrostatic micromotors have demonstrated successes but also uncovered limitations. Problems with these types of motors arise in the areas of friction, fabrication aspect ratio constraints, and low torque-to-speed characteristics.

Flynn *et al.* [11] provide a detailed summary of these problems and propose a piezoelectric ultrasonic micrometer as an alternative approach. This structure, fabricated from thin-film lead zirconium titanate (PZT), circumvents many of the drawbacks of electrostatic micromotors. This paper reports on our experiences with the first prototype motors that we have fabricated.

Our idea is based on the underlying principles of commerically available ultrasonic motors currently popular in Japan [13], [1], [23], and [16], which essentially convert electrical power to mechanical power through piezoelectric interaction. Mechanical power is then coupled to a load through a frictional phenomenon induced by a traveling wave deformation of the material. Piezoelectric motors display distinct advantages over traditional electromagnetic motors such as small size, low noise, and high torque-to-speed ratios. These commercially available motors, however, use PZT in its bulk ceramic form, which must be cut and milled.

Our contribution has been to realize that if PZT can be deposited in a thin-film form compatible with silicon processing, then motors can be manufactured in a batch printing process instead of being individually machined.

Additionally, these motors should show significant improvements in performance over bulk PZT motors. That

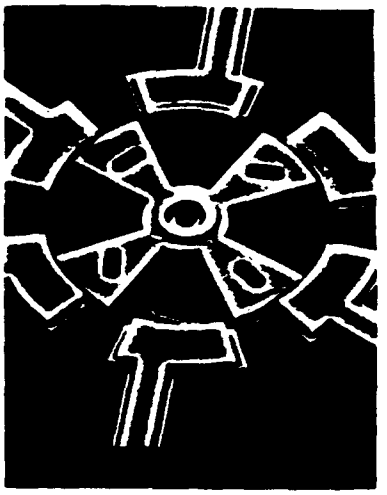

Fig. 1. A variable capacitance motor has a 100 μm diameter rotor which revolves around a bearing as oppositely placed stators are sequentially stepped with the applied drive voltages [25].

Fig. 2. The wobble motor contains a rotor which is attracted to active electrodes as the drive voltages are sequenced around the perimeter, similar to a variable capacitance motor. Since the rotor is the bearing, it tends to "wobble" [14].

is, because the films are very thin it is possible to apply much higher electric fields than in thicker bulk devices. This leads to higher energy densities.

II. Advantages of Piezoelectric Motors

Energy Density—The argument for pursuing piezoelectric ultrasonic micromotors is based on energy density considerations. The maximum energy density storeable in the air gap of an electrostatic micromotor is

$$\tfrac{1}{2}\,\epsilon_{air} E_{bd}^2$$

where E_{bd} is the maximum electric field before breakdown (approximately 10^8 (V/m) for 1 μm gaps) and where ϵ_{air} is the permittivity of air (equal to that of free space).

For a piezoelectric motor made from a ferroelectric material such as PZT, the energy density becomes

$$\tfrac{1}{2}\,\epsilon_{pzt} E_{bd}^2.$$

Thin-film PZT can similarly withstand high electric fields ($E_{bd} \cong 10^8$ V/m), but the dielectric constant is three

orders of magnitude larger ($\epsilon_{pzt} \cong 1300\,\epsilon_0$) than air. Other types of thin-film piezoelectric (but not ferroelectric) ultrasonic actuators have been produced [20] from zinc oxide, but the dielectric constant is only one order of magnitude larger ($\epsilon_{zo} \cong 10\,\epsilon_0$) than air. The greater the energy density stored in the gap, the greater the potential for converting to larger torques, or useful work out.

Low Voltages—Piezoelectric motors are not required to support an air gap. Mechanical forces instead, are generated by applying a voltage directly across the piezoelectric film. Because these ferroelectric films are very thin (ours are typically 0.3 μm), intense electric fields can be established with fairly low voltages. Consequently, we drive our thin-film PZT motors with two or three volts as opposed to the hundred or so volts needed in air-gap electrostatic actuators.

Geardown—Energy density comparisons may be the primary motivators in pursuing PZT micromotors, but there are other advantages as well. Because this strong dielectric material also bends with applied voltage, mechanical power can be coupled out in unique ways. Fig. 3 illustrates an ultrasonic traveling wave motor marketed by Matsushita (Panasonic). Two bulk ceramic layers of PZT are placed atop one another. Each layer is segmented such that neighboring segments are alternately poled. That is, for a given polarity for applied voltage, one segment contracts while its neighbor expands. These two layers are placed atop one another but offset so that they are spatially out of phase. When also driven temporally out of phase, the two piezo layers induce a traveling wave of bending in the elastic body. Any point on the surface of the stator then moves in an ellipse and by contacting a rotor onto the stator, the rotor is pulled along through frictional coupling. Fast vibratory vertical motions are transformed into a slower macroscopic motion tangential to the surface where peak performance is attained at resonance. This geardown means that we can fabricate motors without the need for gearboxes. This is especially important when we compare to electrostatic variable capacitance micromotors, which spin at tens of thousands of revolutions per minute [5]. Gearing down to a useful speed for a robot from such a motor would require a gear several feet in diameter. While electrostatic wobble micromotors are also able to produce an inherent gear reduction, they do not incorporate the advantage of high dielectric materials that the piezoelectric motors possess.

No Levitation—Friction is another major player in problems besetting micromotors. In a variable capacitance electrostatic micromotor, frictionless bearings are something to strive for, as the rotor needs to slide around the bearing. Piezoelectric traveling-wave motors, on the other hand, are based on friction—it is sliding that needs to be prevented. Consequently, there is no need to levitate the rotor, a fact that makes a piezoelectric motor much more amenable to designs for transmitting power to a load. Furthermore, because the rotor in an electrostatic variable capacitance micromotor flies above the stator, it needs to be very flat. Electrostatic micromotors are small, on the order of 100 μm in diameter, because of the difficulties in fabricating large rotors without warpage. In a piezoelectric ultrasonic motor, the rotor is in physical contact with the stator, so the actuator can scale to much larger sizes for resulting higher torques.

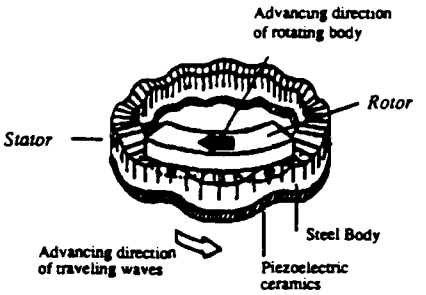

Fig. 3. An electrically induced wave of mechanical deformation travels through a piezoelectric medium in the stator of an ultrasonic motor [21].

Axial Coupling—The consequences of the effects of friction and stability in various types of micromotors force specific geometries on these actuators. Variable capacitance motors require a radial gap design due to stability considerations. That is, the capacitor plates sliding past each other are radially distributed about the bearing. Since silicon processing techniques cannot create large structures in the vertical dimension, that leaves very little area for energy transduction. Similarly, the physics of wobble motors constrains them to have cylindrical coaxial geometries. Ultrasonic motors, however, due to this frictional coupling, can be formed into either linear or rotary motors and in addition, have the advantage that the rotor can sit atop the stator, creating more area over which to couple power out. The large planar area of ultrasonic motors is also symbiotic with planar lithographic techniques.

Rotor Material—Friction coupling (as opposed to charge attraction) leads to another trait characteristic of piezoelectric ultrasonic motors—the rotor can be of any material. That is, the rotor need not be a good conductor as in variable capacitance or wobble motors. Rotor conductivity is unimportant, in contrast to an electrostatic induction micromotor. Most importantly, a piezoelectric ultrasonic motor could actuate a pump, and the fluid can then be *any* solution, without regard to conductivity.

Holding Torque—Finally, in terms of complete systems such as autonomous robots or battery operated machines, total energy consumption over the lifespan of the system is of critical concern. Piezoelectric ultrasonic motors, again due to friction coupling, can maintain holding torque even in the absence of applied power. This is a unique trait for an actuator that does not contain a gearbox, much less a transmission system or a brake.

III. From Materials to Devices

Bulk ceramic PZT has been widely used for decades but thin-film ferroelectrics are new arrivals, having only recently been developed for nonvolatile memory applications [22], [27]. One problem with these new ferroelec-

tric memories is fatigue, as the chips actually *flex* when memory cells switch. But that is exactly the effect we seek to exploit!

We would like films that maximize the piezoelectric effect in order to design useful high torque, low speed micromotors but the leap from materials to devices is a large one. Standing on the shoulders of previous technology is, in general, a good idea (and one that has been the approach in electrostatic micromotor research to this point—some even going so far as to label them "IC-processed micromotors" [24]). Stepping away from known silicon processing techniques and incorporating a new material can be a large undertaking, especially when the aim is to develop a new device. Consequently, the design for the device has to be as simple as possible in terms of materials processing to ensure a reasonable chance of success.[1]

A. Keeping Things Simple

Figs. 4 and 5 illustrate our initial designs for the stators of linear and rotary motors (carriages and rotors have not been microfabricated—at the moment we simply place small glass lenses or other materials down on the stators). A silicon-rich nitride layer is deposited on a silicon wafer and is then patterned on the backside to create a membrane. One hundred twenty stator structures are patterned per two-inch wafer. After the membranes are etched, piezoelectric capacitor structures are built. These structures consist first of a bottom electrode formed from titanium and platinum. The PZT dielectric is then added, and finally the patterned gold top electrodes are deposited. The bottom electrode and thin-film PZT are laid uniformly over the entire wafer, while gold top electrodes are positioned only above membranes.

A close-up of the membrane cross section is shown in Fig. 6. Note that the silicon wafer and the silicon nitride membrane provide only structural support for the stator. No electrical properties or charge attraction effects of silicon are currently used in this motor. Future iterations might find other manufacturing technologies more attractive, but for the present we use silicon for its accompanying tools and lithographic techniques.

These stators were designed in this fashion because the materials requirements here are much simpler than in, for instance, a Panasonic motor (Fig. 3), which would require two layers of ceramics with alternately poled segments throughout each piece. Our microfabricated stators require only one layer of PZT and that layer is poled uniformly everywhere. The trade-off is that our motors now require a four-phase drive to induce a traveling wave, whereas the Matsushita motor requires only two phases. Patterning and wiring is very easy with photolithography. However, while multilayer materials with various geometries of poling are easily realized in macro scale assembled motors, these steps would be very cumbersome from a microfabrication point of view.

[1]Experienced designers usually note, however, that the first way one designs something is always the most complex way [3].

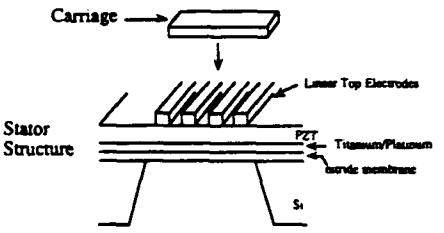

Fig. 4. Linear motors utilizing thin-film PZT are illustrated here. By etching a membrane into a silicon wafer and patterning the stator on the membrane, the stator will be able to deflect more than if it were trying to bend the entire thickness of the wafer. Silicon-rich nitride is used for the membrane. The stator consists of a bottom electrode of titanium and platinum (ground), the PZT film and the patterned gold top electrodes. A carriage would have to be placed down by hand.

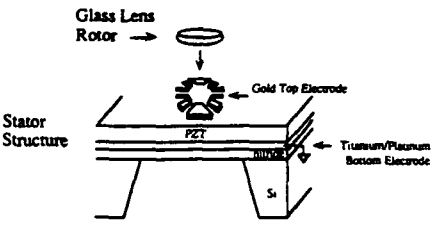

Fig. 5. A rotary motor is made in the same way except that the top electrodes are patterned in a circle. We typically place down a small glass lens for a rotor.

Fig. 6. This scanning electron micrograph shows a cross section of the nitride membrane structure with PZT and the gold top electrode. The titanium-platinum bottom electrode is too thin to see here.

A more recent design is even simpler. We start with thinned wafers which are 75 μm thick (as opposed to the usual 250 μm) and omit membranes entirely. Since stress-free nitride is no longer required as an etch stop to create the membranes, the entire layer sequence just becomes silicon, oxide, Ti-PT, PZT and then gold (titanium is required for adhesion reasons and oxide is necessary to separate silicon from reacting with the PZT).

B. Stators and Rotors

In either case, whether utilizing membraned wafers or thinned wafers, there are a variety of possible geometries for patterning the top electrodes for inducing traveling waves. Fig. 7 shows the simplest layout for a rotary motor. Eight electrodes are patterned radially around a center point and driven four-phase over two wavelengths. Eight probes would be needed to drive the motor in this particular example. However, other patterns on our test wafer use an interconnect scheme between pads to reduce the requirement to four probes. Note in Fig. 7 that there are four extra pads. These can be used as sensors, since the piezoelectric film also is reciprocal, where a bending moment can induce a voltage.

The simplest way to observe electrical to mechanical energy conversion is to place a small object down on the stator as portrayed in Fig. 8. We have found that glass lenses spin the best, although dust particles dance wildly, signaling the onset of resonance as drive frequencies are swept from 50 kHz through several hundred kilohertz. Typical rotational velocities of the glass lens are on the order of 100–300 r/min. One interesting point to note is that four phases are not necessary to induce spinning. In fact, the lenses rotate with only single pad excitation. This is likely due to wave reflections off the edges of the membranes setting up parasitic traveling waves.

In addition to rotary stators, we have fabricated linear stators as shown in Fig. 9. These structures can also be used as surface acoustic wave devices for measuring various properties of the ferroelectric film, such as acoustic velocity, etc.

C. The Process

Nitride membranes are first fabricated using standard bulk micromachining techniques into two-inch silicon ⟨100⟩ wafers. A 1 μm thick low-stress chemical vapor deposition silicon-rich (nonstoichiometric) nitride film acts both as the membrane and the mask for the tetra methyl ammonium hydroxide (TMAH) anisotropic silicon etch. The electroded PZT film (for the stators) is then formed on the membranes. The reduced stiffness of the membranes permit larger stator deflections than would be possible on a full thickness wafer.

Electrode material selection is critical to fully utilize the PZT properties. We have used a 0.46 μm thick platinum layer for our bottom electrode which is deposited on top of a 20 nm titanium adhesion layer. The nitride layer together with the Ti–Pt layers act as a separation barrier preventing the silicon from reacting with the PZT.

Sol-gel PZT film is deposited by a spin-on technique in a series of steps. These films have been characterized as reported in [28] and show some significant improvements over bulk PZT, including a greater breakdown strength and dielectric constant. Although thin-film PZT was first developed for memory devices, much of that work has focused on sputtering and chemical vapor deposition methods, even though it is very difficult to get correct the PZT makeup with these techniques. Sputtering from three separate elementary targets (or even from a single ceramic PZT target) to get lead, zirconium, and titanium atoms all

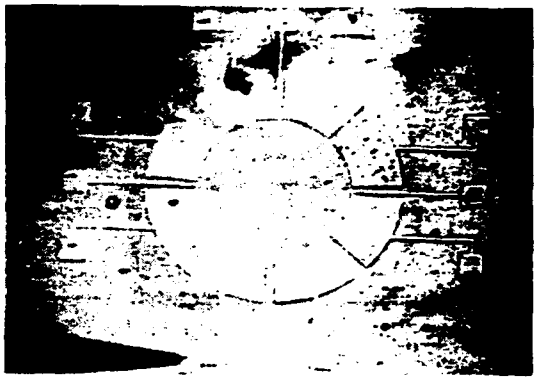

Fig. 7. This eight-pole stator has an inner-diameter of 1.2 mm and an outer diameter of 2 mm placed over a 2.2 mm × 2.2 mm square membrane. The eight pads are driven in a four phase sequence (sin, cos, −sin and −cos), repeated twice. The extra four pads at the north, east, south and west positions are undriven pads which can be used as passive piezoelectric sensors. That is, a signal will be generated as the wave passes through the pad.

Fig. 8. Here a plano-convex 1.5 mm diameter glass lens is placed convex surface down upon a rotary stator which has the same dimensions as Fig. 7. Although there is no bearing, the lens spins at 100–300 r/min when the stator is driven at 90 kHz.

Fig. 9. Linear stators have also been fabricated. Here, the probe pads to the right are 200 μm square and connect to every fourth electrode for setting up four-phase traveling waves. These structures are patterned over similarly shaped linear membranes.

in their proper atomic positions in the crystal lattice is significantly harder than preparing a solution of the proper composition and spinning it onto a wafer as in a sol-gel process. These sol-gel fabricated films do, in fact, exhibit the proper perovskite structure and show strong ferroelectric characteristics. For memory applications, piezoelectric flexing is not of interest, but the conformal coating properties of vapor desposited films are of interest. Sol-gel films, on the other hand, are planarizing, which can be a problem where uniform thicknesses even over undulating surfaces are required. One critical requirement for preparing quality sol-gel films is cleanliness, as wet spin-on techniques are more susceptible to the particle contamination than vacuum-based methods.

The sol mixture is prepared from the lead precusor, lead acetate trihydrate, together with alkoxides of Ti and Zr in 2-methoxyethanol as the solvent. Films are spun-on in approximately 50 nm layers. The film is pyrolyzed under quartz lamps after each step to remove organics. After six to eight layers, the film is annealed to crystallize into the perovskite phase, which is the type of crystalline form which brings out the strong ferroelectric and piezoelectric traits. Annealing is carried out above 500 C. These PZT films are of the 52–48 mole ratio of Zr–Ti, which places them on the morphotropic phase boundary. The morphotropic phase boundary composition is that composition for which the crystallites have the maximum number of possible domain states because the composition lies at the boundary of the tetragonal phase (six possible domain states) and the rhombohedral phase (eight possible domain states). This position among the possible spectrum of compositions in the lead zirconate–lead titanate solid solution system is the most amenable for attaining the distinctive ferroelectric properties. One interesting point about these thin films of PZT, in contrast to its bulk form, is that poling, the process of aligning domains in order to bring out these strong ferroelectric characteristics, no longer needs be performed at elevated temperatures.

Characteristic measurements, described in more detail in [27] are summarized in Table I. Similar measurements reported in the literature for bulk PZT [15] yield some interesting comparisons. The breakdown field strength 1 MV/cm is significantly improved over bulk PZT, which is often on the order of 40 kV/cm. Our sol-gel PZT films also exhibit almost twice the relative dielectric constant, 1300, of (similarly undoped) bulk PZT, which is 730.

Once the PZT film has been annealed, 0.5 μm thick gold electrodes are deposited and patterned by lift-off. A variety of eight- and 12-pole rotary stators on three sizes of square membranes (0.8, 2.2, and 5 mm per side) and various configurations of linear stators are patterned.

The structures built on thinned wafers are fabricated in an analogous manner except that the membrane etch is skipped and 0.5 μm oxide is used in place of nitride. The oxide layer together with the titanium–platinum layer act as a separation barrier preventing the silicon from reacting with the PZT.

TABLE I
SOL-GEL PZT FILM CHARACTERISTICS

E_{bd}	1 MV/cm	Breakdown field
ϵ_{pzt}	$1300\epsilon_o$	Dielectric constant
$\tan\delta$	0.03	Loss tangent
d_{33}	220 pC/N	Long. piezoelectric coefficient
d_{31}	−88.7 pC/N	Trans. piezoelectric coefficient
P_r	36 μC/cm^2	Remanent polarization
k_{33}	0.49	Long. coupling factor
k_{31}	0.22	Trans. coupling factor
k_p	0.32	Planar coupling factor

V. RESULTS

Initial experiments with these thin-film PZT actuators have raised some intriguing questions. On the one hand, we have observed phenomena we expected such as high energy densities, gear down, and low voltage operation. A 4 V peak-to-peak drive signal at 90 kHz competently spins a fairly large rotor, a glass lens 1.5 mm in diameter, at 100–300 r/m. On the other hand, the lens spins competently with only one phase excitation, and does not spin any better with four, something we did not expect! Furthermore, changing directions when applying four-phase drive does not cause the rotor to reverse, although in one instance, it did cause the lens to stop. Essentially, we are not inducing traveling waves in the manner we would like, but evidently there is enough energy density that the lenses spin anyway.

We have observed other indications of high energy density. Not only do dust and particles vibrate across the stators upon resonance, but in certain instances in which a pad's impedance is very low, applying a voltage on the order of 10 V will cause a static deflection dependent on voltage that can be seen through the microscope as a darkened area where the surface is deformed and reflecting light away from the eyepiece. An example with a unique stress pattern is shown in Fig. 10. Note that even at 10 V, the electric field that we can apply across our 0.3 μm thick films contribute to energy densities well beyond those achievable with bulk ceramic PZT motors.

The single phase drive is intriguing and brings into question the effects of the boundary conditions on the waves imposed by the edges of the membranes. At high enough frequencies (several hundred kilohertz) standing waves become visible on both linear and square membranes. Rotors continue to spin, however, even though the motors are not working in the manner in which they were designed. The plano-convex glass lenses seem to spin because the contact is a point. We have observed glass lenses, convex side down, jiggling across the stator until brushing up against the inner radius of the gold electrodes which are approximately 0.5 μm tall, whereupon they sit and spin. We have also observed that plano-convex lenses flat side down do not spin, nor do annularly shaped objects such as jeweled bearings.

In this first fabrication sequence, we made no attempt to microfabricate a bearing or etch a rotor in place. Con-

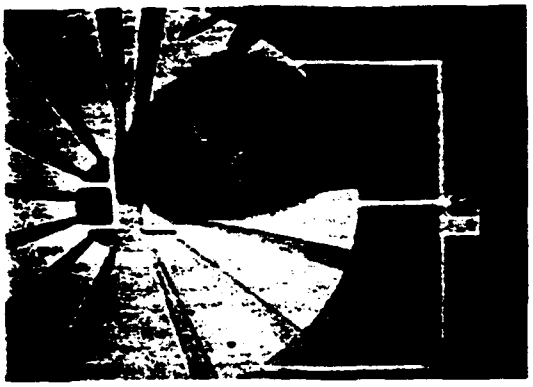

Fig. 10. Static deflection of this partially short stator pad can be seen through the microscope. The darkened portion is deformed, deflecting light away from the eyepiece. 10V are applied from the electrode at the right across the PZT, to the ground plane beneath it.

sequently, the amount of frictional coupling is only determined by the weight of the rotor. In fact, it is possible there is no frictional coupling and the lens is merely sliding on air as the surface vibrates. Nevertheless, a mass is spinning and it is possible to calculate a torque by measuring the inertia of the lens and its acceleration when starting. Approximating our lens as a disk 1 mm thick and estimating from visual observation that it reaches a final velocity of 3 Hz in a quarter of a second, the resulting torque is 41 pNm. We can compare to variable-capacitance electrostatic micromotors by normalizing over voltage squared, which gives a figure of merit over a class of experiments. This normalized net torque for such electrostatic micromotors (typically run at 100 V) is 1.4×10^{-15} Nm/V^2. The figure of merit for our piezoelectric motors then becomes, for 5 V excitation, 1.6×10^{-12} Nm/V^2, about three orders of magnitude larger. What this number actually signifies for a piezoelectric motor with no bearing and no traveling wave drive is debatable. Mostly, it serves to underscore that the films are indeed very active, encapsulate high energy densities and can move fairly large objects with low voltages.

True motor action will depend on future attempts to fabricate a bearing and to measure torques across a spectrum of normal forces. Further experiments are needed to determine better structures for guiding traveling waves. Instruments need to be developed for visualizing the waves throughout a spectrum of frequencies and for ascertaining the amplitudes of these dynamic deflections. Determining proper rotor-stator interface coatings for high friction contact would also be helpful.

V. Conclusion

Electrostatic motors are essentially the duals of magnetostatic motors, which have been around for years and are well understood. Piezoelectric ultrasonic motors, on the other hand, are fairly new and ferroelectric thin films are newer still. Many factors conspire to produce complexities and difficulties in analyzing these structures: nonlinear materials, coupled electrical and mechanical fields, resonance drives, clamped and unclamped waveguide boundary conditions and friction based interactions between rotors and stators, to name a few. Building mass-producible useful-torque-producing micromotors will be hard. Building complete gnat robots will be much harder. But the payoff will be enormous.

Acknowledgment

The authors would like to thank Chester Bukowski of MIT Lincoln Laboratory for his advice and assistance with the silicon fabrication and micromachining of these motors.

References

[1] Y. Akiyama, "Present state of ultrasonic motors in Japan," *JEE*, Apr. 1987.
[2] C. M. Angle, "Genghis, a six legged autonomous walking robot," S.B. thesis, Massachusetts Inst. Technol., Cambridge, 1989.
[3] C. M. Angle, Personal communication, MIT Artificial Intelligence Lab., Cambridge, MA, 1990.
[4] S. F. Bart, T. A. Lober, R. T. Howe, J. H. Lang, and M. F. Schlecht, "Design considerations for microfabricated electric actuators," *Sensors and Actuators*, vol. 14, no. 3, pp. 269-292, 1988.
[5] S. F. Bart, M. Mehregany, L. S. Tavrow, J. H. Lang, and S. D Senturia, "Measurements of electric micromotor dynamics," in *Microstructures, Sensors & Actuators*, ASME, DSC-vol. 19, pp. 19-29, Nov. 25-30, 1990.
[6] R. A. Brooks, "A robust layered control system for mobile robot," *IEEE J. Robotics Automat.*, vol. RA-2, pp. 14-23, Apr. 1986
[7] ——, "A robot that walks: emergent behavior from a carefully evolved network," *Neural Comput.*, vol. 1, 1989.
[8] J. H. Connell, *Minimalist Mobile Robotics—A Colony-style Architecture for an Artificial Creature*. San Diego, CA: Academic, 1990.
[9] A. M. Flynn, "Gnat robots (and how they will change robotics)," presented at *IEEE Micro Robots and Teleoperators Workshop*, Hyannis, MA, Nov. 1987.
[10] A. M. Flynn, R. A. Brooks, W. M. Wells III and D. S. Barrett, "Intelligence for miniature robots," *J. Sensors Actuators*, vol. 20, pp. 187-196, 1989.
[11] A. M. Flynn, R. A. Brooks, and L. S. Tavrow, "Twilight zones and cornerstones: A gnat robot double feature," MIT Artificial Intelligence Lab., Cambridge, MA, Memo 1126, July.
[12] H. Fujita, A. Omodaka, M. Sakata and Y. Hatazawa, "Variable gap electrostatic actuators," in *Tech. Dig. 8th Sensor Symp.*, 1989, pp. 145-148.
[13] R. Inaba, A. Tokushima, O. Kawasaki, Y. Ise, and H. Yoneno, "Piezoelectric ultrasonic motor," in *Proc. IEEE Ultrason. Symp.*, 1987, pp. 747-756.
[14] S. C. Jacobsen, R. H. Price, J. E. Wood, T. H. Rytting and M. Rafaelof, "The wobble motor: An electrostatic, planetary armature, microactuator," in *Proc. IEEE Micro Electro Mech. Syst.*, Salt Lake City, UT, Feb. 20-22, pp. 17-24.
[15] B. Jaffe, W. R. Cook, and H. Jaffe, *Piezoelectric Ceramics*. New York: Academic, 1976.
[16] A. Kumada, "Piezoelectric revolving motors applicable for future purpose," Seventh Int. Symp. Appl. Ferroelectrics, Urbana-Champaign, IL, June 6-8, 1990.
[17] P. Maes and R. A. Brooks, "Learning to coordinate behaviors," in *Proc. 1990 Amer. Assoc. Artificial Intelligence Conf.*, Aug. 1990.
[18] M. J. Mataric, "Environment learning using a distributed representation," IEEE Robotics Automat., Cincinnati, OH, May 1990.
[19] M. Mehregany, S. F. Bart, L. S. Tavrow, J. H. Lang and S. D Senturia, "Principles in design and microfabrication of variable-capacitance side-drive motors," *J. Vacuum Sci. Technol.*, vol. A8, no 4, pp. 3614-3624, July-Aug. 1990.
[20] R. M. Moroney, R. M. White, and R. T. Howe, "Ultrasonic micromotors," presented at IEEE Ultrason. Symp., Montreal, Canada, Oct 1989.

[21] Panasonic Tech. Ref., "Ultrasonic motor," 1987.
[22] Ramtron Corp., "Nonvolatile ferroelectric technology and products," Colorado Springs, CO, Tech. Rep., 1988.
[23] Shinsei Corp., "A new concept in motors: Ultrasonic wave oscillation drive energy," Shinsei Corp., May 1988.
[24] Y. C. Tai, L. S. Fan, and R. S. Muller, "IC-processed micro-motors: Design, technology and testing," in *Proc. IEEE Micro Electro Mech. Syst.*, Salt Lake City, UT, Feb. 20-22, pp. 1-6.
[25] L. S. Tavrow, "A LOCOS-based microfabricated radial-gap electric motor," Ph.D. dissertation, Massachusetts Inst. Technol., Cambridge, MA, Feb. 1991.
[26] W. Trimmer and R. Jebens, "An operational harmonic electrostatic motor," *Proc. IEEE Micro Electro Mech. Syst.*, Salt Lake City, UT, Feb. 20-22, pp. 13-16.
[27] K. R. Udayakumar, J. Chen, S. B. Krupanidhi and L. E. Cross, "Sol-Gel derived PZT thin films for switching applications," in *Proc. 7th Int. Symp. Appl. Ferroelect.*, Urbana-Champaign, IL, June 6-8, 1990.
[28] K. R. Udayakumar, S. F. Bart, A. M. Flynn, J. Chen, L. S. Travrow, L. E. Cross, R. A. Brooks and D. J. Ehrlich, "Ferroelectric thin film ultrasonic micromotors," in *Proc. Fourth IEEE Workshop Micro Electro Mech. Syst.*, Nara, Japan, Jan. 30-Feb 2, pp. 109-113.

Anita M. Flynn (S'80-M'84-S'84-M'85-S'86-M'87) received the B.S. and M.S. degrees in electrical engineering from the Massachusetts Institute of Technology, Cambridge, in 1983 and 1985, respectively.

Subsequent to that, she spent five years as a Research Scientist at the MIT Artificial Intelligence Laboratory in the Mobile Robotics Group working on sensing and control problems in autonomous robots. Since 1990 she has been a Ph.D. student at the Artificial Intelligence Laboratory researching piezoelectric motors for miniature robots.

Lee S. Tavrow (S'85-M'86-S'86-M'90) received the B.S., M.S., and Ph.D. degrees in electrical engineering from the Massachusetts Institute of Technology, Cambridge, in 1987, 1987, and 1991, respectively.

During 1986-1987 he was employed by DEC, Hudson, MA, where he worked on analog and mixed-signal VLSI. In 1991 he joined Sun Microsystems Laboratories, Mountain View, CA, where he is currently involved with VLSI and CAD. His principal research interests include digital and analog VLSI, CAD, microfabrication, and electromechanics.

Dr. Tavrow is a member of Tau Beta Pi and Eta Kappa Nu.

Stephen F. Bart (S'84-S'88-M'88-M'90) received the B.S., M.S., and Ph.D. degrees in electrical engineering from the Massachusetts Institute of Technology, Cambridge, in 1982, 1986, and 1990, respectively.

In 1991, he joined Bose Corporation where he is currently involved in sensing and active control of complex electromechanical systems. His research has involved the electromechanics and fluid mechanics of biological tissues, pollution control devices, and microfabricated actuators. His research interests include the dynamics and control of lumped and continuous electromechanical systems with application to both macroscopic and microfabricated devices.

Dr. Bart is a member of Eta Kappa Nu, Tau Beta Pi, and Sigma Xi.

Rodney A. Brooks (M'84) received the M.Sc. degree in mathematics from Flinders University, South Australia, and the Ph.D. degree in computer science from Stanford University, Stanford, CA.

He is an Associate Professor of Electrical Engineering and Computer Science at the Massachusetts Institute of Technology, Cambridge. At MIT he is the Director of the Mobile Robot Group in the Artificial Intelligence Laboratory. Small insect-like robots he has designed have received international recognition. He serves as a consultant in computer sciences and robotics, and is a member of the editorial boards for numerous publications. Dr. Brooks is a fellow of the American Association of Artificial Intelligence.

Daniel J. Ehrlich (A'90) received the Ph.D. degree in optics from the University of Rochester, Rochester, NY, in 1977.

In 1977 he joined the MIT Lincoln Laboratory, Lexington, and subsequently has held assignments as Technical Staff in the Quantum Electronics Group, Assistant Leader of the Microelectronics Group, and Leader of the Submicrometer Technology Group. He is currently a Senior Staff member in the Solid State Division. He has worked on laser fusion, the invention of new lasers, and laser applications in microelectronics including new submicrometer lithographies and pattern transfer technologies. He is currently working on the application of microfabrication technology to biology and miniaturized electromechanics. He is author of 12 issued patents and more than 150 refereed journal publications in laser applications and microfabricaton.

K. R. Udayakumar was born in Bangalore City, India. He received the B.S. degree in physics from Bangalore University, Bangalore, India, and the Master's degree in ceramic engineering from the New York State College of Ceramics, Alfred, NY, in 1987. He is currently working toward the Ph.D. degree in solid state science at the Materials Research Laboratory, Pennsylvania State University. He worked as a Scientist for a year at the Defence Research Laboratory at Hyderabad, India. In 1988, he joined the Materials Research Laboratory of the Pennsylvania State University, University Park, and is working toward the Ph.D. degree in solid state science. His Ph.D. thesis involves the fabrication and characterization of novel ferroelectric thin films for applications in non-volatile memories, DRAM's, and piezoelectric micromotors. His major areas of interest broadly include ferroelectric thin films, energetics of point defects, and thermodynamics of solids and chemical processes.

L. Eric Cross (SM'79-F'84) received the B.Sc. (hons.) degree in physics from Leeds University in 1948 and the Ph.D. degree in physics in 1953. He was a University Scholar, an Assistant Professor, and an ICI fellow at the University of Leeds. After a short period at the Electrical Research Association in Leatherhead Surrey, he moved to the USA to take up a position at the developing Materials Research Laboratory (MRL) at Pennsylvania State University, University Park. He was for many years an Associate Director of MRL, and was the Laboratory Director from 1985 to 1989. He is now an Evan Pugh Professor of Electrical Engineering at Pennsylvania State University.

His interests are in dielectric and ferroelectric crystals; piezoelectric and electrostrictive ceramics; composites for sensor, actuator and transducer applications, and as components in "smart" materials and structures. He has co-authored more than 300 technical papers, and sections of six books.

Dr. Cross is a member of the National Academy of Engineering, a Fellow of the American Institute of Physics, of the American Ceramic Society, and the American Optical Society, and a member of the Japanese Physical Society. He is chairman of the IEEE Committee on Ferroelectrics, U.S. representative for ferroelectrics on IUPAP, and a member of the Defense Sciences Research Council of DARPA.